
**TRIBHUVAN UNIVERSITY**

**INSTITUTE OF ENGINEERING**

**PULCHOWK CAMPUS**

**THESIS NO.: M-69-MSMDE-2019-2023**

# Design Optimization of Bovet Based Micro Francis Turbine Used in Sand Laden Water

**by**

**Neeraj Adhikari**

**A THESIS**

**SUBMITTED TO THE DEPARTMENT OF MECHANICAL AND AEROSPACE ENGINEERING IN PARTIAL FULFILLMENT OF THE REQUIREMENTS FOR THE DEGREE OF MASTER OF SCIENCE IN MECHANICAL SYSTEM DESIGN AND ENGINEERING**

**DEPARTMENT OF MECHANICAL AND AEROSPACE ENGINEERING**

**LALITPUR, NEPAL**

**OCTOBER, 2023**

## COPYRIGHT

**TRIBHUWAN UNIVERSITY**

**INSTITUTE OF ENGINEERING**

**PULCHOWK CAMPUS**

**DEPARTMENT OF MECHANICAL AND AEROSPACE ENGINEERING**

The undersigned certify that they have read, and recommended to the Institute of Engineering for acceptance, a thesis entitled "**Design optimization of Bovet based micro Francis used in sand laden water**" submitted by Neeraj Adhikari in partial fulfillment of the requirements for the degree of Master of Science in Mechanical System Design and Engineering.

_____

Supervisor, Prof. Dr. Tri Ratna Bajracharya
Professor
Department of Mechanical and Aerospace Engineering, Pulchowk Campus

_____

External Examiner, Dr. Sailesh Chitrakar
Assistant Professor
Kathmandu University

_____

Committee Chairperson, Dr. Sudip Bhattarai
Head of Department
Department of Mechanical and Aerospace Engineering, Pulchowk Campus

2023/09/26
Date of Final Defense

## ABSTRACT

The Francis turbine is a highly prevalent choice in hydropower generation in Nepal due to its capacity to operate efficiently across a wide range of conditions i.e. large domain of head and flow rate. Traditional design techniques, such as the Bovet method, rely on empirical equations to determine the turbine's meridional profile based on hydrological factors which can be further optimized. Evaluating the runner's performance involves considering factors such as efficiency, resistance to cavitation, erosion resistance, part load performance and more. To enhance a turbine's performance for a specific site, it can be optimized by adjusting various design parameters.

In this research optimization of Francis runner was conducted in three steps. Initially optimization of size of meridional profile was done. In this initial phase optimization was performed on the basis of obtained runner efficiency. After obtained runner of best meridional profile, lean angle of the runner was varied from $-10^{o}$ to $10^{o}$. $-5^{o}$ lean angle has performed best on the basis of efficiency. Then taking the runner design 600 design samples were created using Latin Hypercube Sampling (LHS) techniques. For obtaining 600 design points shape of leading edge, training edge, hub, shroud and beta angle distribution were varied. After running CFD simulation for all design points 578 were successful and obtained results were used to train neural network which was coupled with genetic algorithm to find the optimal design based on objective function.

In the optimized design, the outcomes indicate that the most significant improvements were observed in the reduction of cavitation, which decreased by 99% compared to the initial design. There were minor enhancements in shaft power (0.2%) and efficiency (1.3%). Additionally, the tendency for erosion was reduced by 18%, and the objective function value decreased by 28% in comparison to the initial design.

## ACKNOWLEDGEMENT

I would like to acknowledge Professor Dr. Tri Ratna Bajracharya of the Institute of Engineering for his continuous and invaluable guidance throughout the completion of my work. His timely guidance, encouragement, intellectual insights, and scientific attitude all contributed to the successful completion of my thesis.

I am particularly grateful to Prof. Dr. Laxman Poudyal, M.Sc. in Mechanical System Design and Engineering Coordinator, and all of the excellent faculty members for their continual encouragement, support, and direction throughout this study. In addition, I would like to express my gratitude to the faculty and staff of the Department of Mechanical and Aerospace Engineering for their assistance throughout my academic career.

The University Grant Commission Nepal funded this study with Faculty Research Grant number FRG-77/78-Engg-I. I'd also want to acknowledge the Nepal University Grant Commission for their support. I'd also want to thank my co-investigator, Asst. Prof. Laxman Motra, The work carried out by Binaya Lamichhane during his graduate thesis and by Srijan Satyal, Samundra Karki, Prasanna Koirala, and Krishna Prasad Rijal during their undergraduate project has been continued with this research. For all of their earlier works, I therefore want to thank them.

I'd want to admire my colleagues and mentors for their helpful advice, expertise, support, and helpful feedback, all of which have aided my development. I'd want to thank Suman Acharya, Krishna Bhattarai, Prabin Dhakal, and Sushsant Chalise in particular for keeping me encouraged throughout the process.

Finally, I would like to express thanks to all persons, both directly and indirectly involved, who contributed to the successful completion of this thesis work.

Neeraj Adhikari
075MSMDE013
M.Sc. in Mechanical System Design and Engineering

## TABLE OF CONTENTS

## LIST OF FIGURES

## LIST OF TABLES

## LIST OF SYMBOLS

| | |
|---|---|
| $Q$ | Volume Flow Rate |
| $C_{m1}/C_{m2}$ | Meridional velocity at runner inlet and outlet |
| $R_1/R_2$ | Radius of runner inlet and outlet |
| $B_1$ | Height of runner at inlet and outlet |
| $D_1/D_2$ | Diameter of the runner at inlet and outlet |
| $C_1/C_2$ | Absolute velocity at inlet and outlet |
| $C_{U1}/C_{U2}$ | Whirl velocity at inlet and outlet |
| $W_1/W_2$ | Relative velocity at inlet and outlet |
| $U_1/U_2$ | Peripheral velocity at inlet and outlet |
| $G$ | Acceleration due to gravity |
| $\beta_1/\beta_2$ | Blade inlet and outlet angle |
| $P_t$ | Power transferred to thee runner |
| $H$ | Net head |
| $\eta$ | Efficiency |
| $P_a$ | Power available |
| $N$ | Rotational speed (rpm) |
| $n_o$ | Specific speed |
| $\overline{u_\iota' u_\jmath'}$ | Reynolds stress tensor |
| $\delta_{ij}$ | Kronecker delta |
| $\nu_t$ | Eddy viscosity |

| | |
|---|---|
| $\theta$ | Lean angle |
| $W_\eta$ | Weight for efficiency term |
| $W_h$ | Weight for head term |
| $W_e$ | Weight for erosion term |
| $W_c$ | Weight for cavitation area |

## LIST OF ACRONYMS AND ABBREVIATIONS

| | |
|---|---|
| AEPC | Alternate Energy Promotion Centre |
| ANN | Artificial Neural Network |
| ATM | Adaptive Tetrahedral Meshing |
| CAD | Computer Aided Design |
| CFD | Computational Fluid Dynamics |
| DNS | Direct Numerical Solution |
| DOE | Design of Experiments |
| GA | Genetic Algorithm |
| kW | Kilo Watts |
| LES | Large Eddy Simulation |
| LHS | Latin Hypercube Sampling |
| MOGA | Multi Objective Genetic Algorithm |
| MW | Mega Watts |
| NEA | Nepal Electricity Authority |
| NHE | Nepal Hydro & Electric Limited |
| OF | Objective Function |
| RANS | Reynolds Average Navier-Stokes |
| ReLU | Rectified Linear Unit |
| RSM | Reynolds Stress Modeling |

| | |
|---|---|
| SST | Shear Stress Transport |

# CHAPTER 1: INTRODUCTION

## 1.1 Background

Nepal's energy sector plays a vital role in economic development, but challenges persist with inadequate and unreliable electricity supply, primarily reliant on traditional sources like fuel wood. Despite some improvements, the majority of citizens still face partial energy access, with electricity consumption far below global averages. Limited domestic resources and heavy reliance on imported fossil fuels contribute to ongoing energy constraints.

Nepal possesses abundant water resources including snow cover, rivers, springs, lakes, and groundwater. Notably, the country's 6,000 rivers and rivulets are of utmost importance, serving various needs and holding immense potential for hydropower generation due to the nation's rugged topography(Sangroula 2009). The Pharping Hydropower Plant, established in 1911, holds historical significance as Asia's oldest hydropower facility and Nepal's inaugural one. Its construction initiated in 1907 and concluded with commissioning in 1911. Its installed capacity was 500 kW. Nepal's initial hydropower capacity started at 500 kW, but the grid-connected capacity has now surged to nearly 2600 MW. By 2067 B.S., total generation had reached around 600 MW, with recent growth in the sector substantially boosting hydropower output. The Nepal Electricity Authority (NEA) reports an annual addition of approximately 500 MW to the national grid, with ambitions to achieve a total capacity of 10,000 MW in the next five years(R. S. Shrestha et al. 2018).

However, this projected growth poses challenges in reconciling the interests of a robust local hydro engineering industry with those of external contractors and sources of finance. Additionally, the importation of generation and distribution equipment, along with electrical appliances, presents a hurdle. Currently, hydro mechanical industries are producing turbine runners for sub-1 MW projects, with the logical progression being the production of equipment for the small to medium hydro (1 to 100 MW) range. In parallel, Nepal should consider entering the production of electro-mechanical equipment such as generators, potentially through collaborations with foreign industries(R. S. Shrestha et al. 2018).

## 1.2 Problem Statement

Nepal's local hydro mechanical industry predominantly manufactures Cross Flow, Turgo, and Pelton turbines. A research study indicates that the most suitable turbine for Nepal is the Francis turbine. The study analyzed ongoing and planned projects, revealing that 75% of required turbines for hydropower are Francis turbines. Notably, 50% of these Francis turbines are designed for capacities under 5 MW, and 80% are designed for capacities under 25 MW offering substantial prospects for Nepal's hydro mechanical industry, which is primarily centered on Francis turbines(Panta et al. 2014). This turbine's adaptability to a wide range of head and flow rates makes it a fitting choice, with its design being tailored to site-specific conditions. The research aims to propose a design methodology specifically for Francis turbines, focusing on micro hydro applications in Nepal.

The Alternate Energy Promotion Centre (AEPC) states that the total installed capacity at the micro and mini hydro level through 2015–16 is 54.27 MW.(R. S. Shrestha et al. 2018) There's no reason to believe that the popularity of this off-grid electricity source won't keep growing quickly. In addition to employing Nepali equipment and skills to install this hydropower, Nepali businesses are currently supplying and installing hydropower in other neighboring countries.

For Nepal to gain economic advantages from backward linkages, it's essential that the country manufactures or creates equipment within its borders. While a few companies like Nepal Hydro & Electric Limited (NHE) can produce and provide most hydro-mechanical equipment, turbine runners are an exception. Unfortunately, Nepal doesn't have any local manufacturers producing large generators in the electro-mechanical category.

## 1.3 Objectives

### 1.3.1 Main Objective

The main objective of this research is design optimization of Bovet based micro Francis Turbine used in sand laden water

### 1.3.1 Specific Objectives

Listed below are specific objectives

- Reference Design of Francis turbine using Bovet method

- Parametric size optimization of meridional profile obtained using Bovet method
- Parametric lean angle optimization of runner
- To obtain optimized Meridional shape using Meta-model and Genetic Algorithm

### 1.4 Limitations

Following are the scope and limitation of the research

- The data generation and validation of obtained designs are based on steady-state CFD simulation
- As number of simulations are large so much details on the mesh is ignored, automated mesh option of TurboGrid is used
- Materials properties and manufacturing details are not considered
- For each design inlet angle should have been changed accordingly but due to large number of simulation a single inlet angle was used for all the designs

# CHAPTER 2: LITERATURE REVIEW

## 2.1 Francis Turbine

Turbine is the heart of hydropower which extracts energy from water. There exists different turbines namely Francis, Pelton, Kaplan, Cross flow, Turgo, Propeller etc. which can be categorized into impulse and reaction type of turbine. In impulse turbine all of the energy is converted into kinetic energy at the nozzle and no pressure changes occurs through the vanes of the runner. In the case of reaction turbine there is change in both kinetic and pressure energy throughout the runner.

Figure 2.1: Runner of small Francis turbine

Francis is most used turbine in Nepal due to its ability to work under higher domain of head and flow rate. It works under low head to high head and from low flow rate to high flow rates. Spiral casing, Stay vanes, guide vanes, runner and draft tubes are different components of Francis turbine. Water enters the turbine through the spiral casing. The diameter of the casing gradually reduces so that the velocity of water striking the runner blades is uniform. The water from the spiral casing goes through the stay vanes which direct the water to the guide vanes. The guide vanes are used to control the rate of flow of water to the turbine. The angle of the guide vanes can be controlled with the help of a regulating mechanism that affects the magnitude of radial and tangential velocity of water striking the runner blade. The water from the exit of the guide vane strikes the leading edge of the runner blade. The runner is the most important part of the turbine where the pressure and kinetic energy of the water is converted to

mechanical energy as water flows through the blade from the radial direction at the inlet to the axial direction at the outlet.

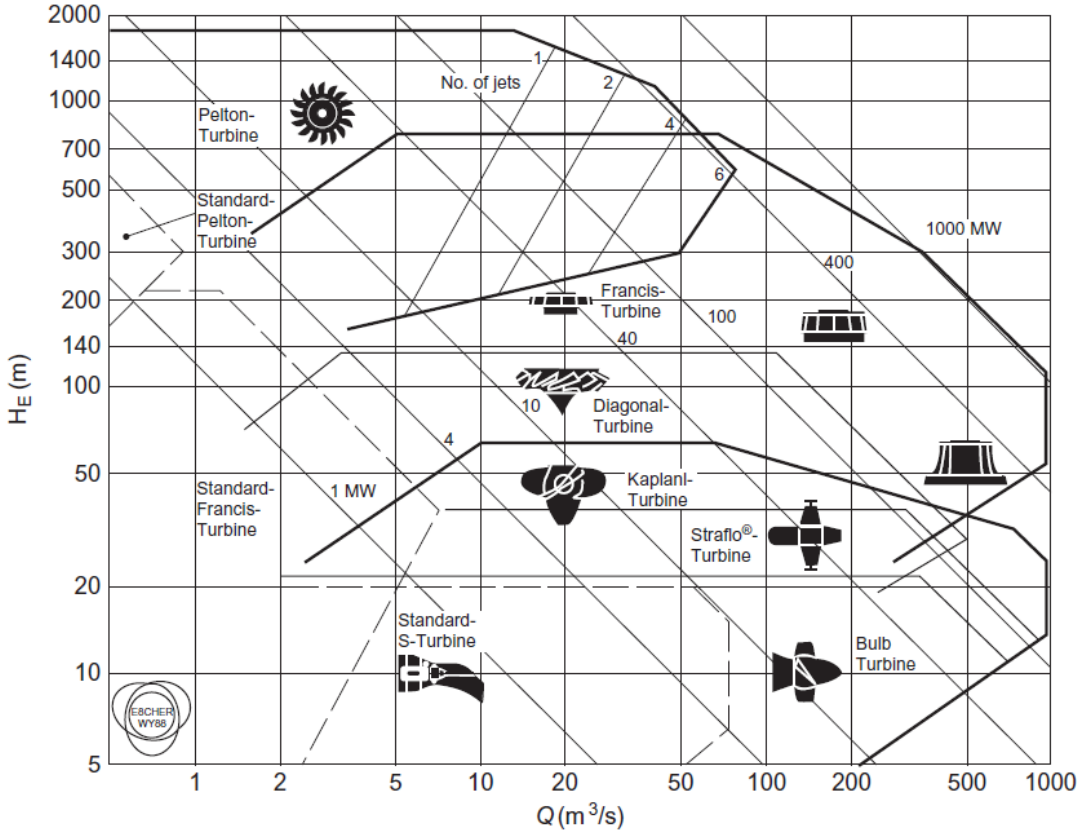


Figure 2.2: Application ranges for various types of hydraulic turbines

## 2.2 Velocity Triangle of Francis Turbine

The volume flow Q through turbine can be expressed as

$$Q = C_{m1} 2\pi R_1 B_1$$

Where $C_{m1}$ is Meridional velocity at runner inlet, $B_1$ is height of the runner inlet and $R_1$ is the radius of runner inlet.

Similarly at outlet of turbine runner,

$$\mathrm{Q} = \frac{\pi}{4} \mathrm{D}_2^2 \mathrm{C}_{\mathrm{m2}}$$

Where $D_2$ is the diameter of the outlet of runner

In the given velocity triangle in figure 2.3, $C_1, C_{u1}, W_1, U_1$ and $C_2, C_{u2}, W_2, U_2$ are the

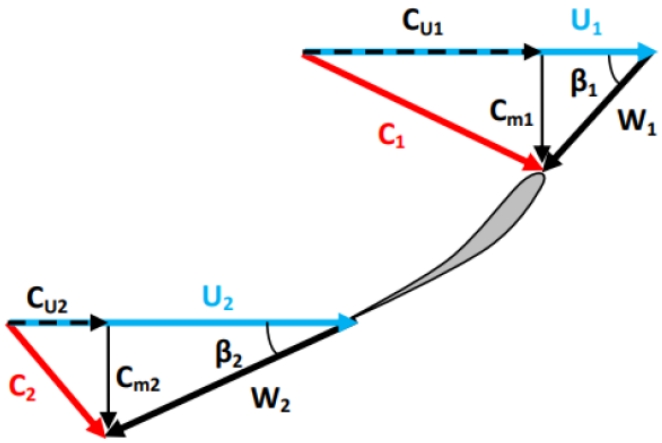


Figure 2.3: Velocity triangle (Gjøsæter 2011)

absolute velocity of flow, tangential/whirl velocity of flow, relative velocity and peripheral velocity at inlet and outlet respectively.

The peripheral velocity of runner at the outlet is

$$U_2 = \frac{2\pi R_2 N}{60}$$

Where $R_2$ is radius from the axis of rotation to different streamlines from hub to shroud in the trailing edge.

For the maximum efficiency whiling velocity at the outlet is set to zero ($C_{u2}$=0).

The outlet angle $\beta_2$ is given by

$$tan\beta_2 = \frac{C_{m2}}{U_2} = \frac{\frac{Q}{\pi R_{2e}^2}}{U_2}$$

$$U_1 = \frac{2\pi R_1 N}{60}$$

$$C_{u1} = \frac{gh}{U_1}$$

The inlet angle $\beta_1$ is given by

$$tan\beta_1 = \frac{C_{m1}}{U_1 - C_{u1}}$$

$$cot\beta_1 = \frac{U_1 - C_{u1}}{C_{m1}} = \frac{2\pi R_{1e} B_1}{Q}\left(\frac{2\pi R_1 N}{60} - \frac{60gH}{2\pi R_1 N}\right)$$

The power transferred to the runner is

$$P_t = \rho Q(U_1 C_{u1} - U_2 C_{u2})$$

The total available power is

$$P_{av} = \rho Q g H$$

Finally Euler turbine equation is

$$\eta = \frac{P_t}{P_{av}} = \frac{U_1 C_{u1} - U_2 C_{u2}}{\rho Q g H}$$

There exists different velocity triangles for different runner and based on velocity triangles. Mainly there are three types of inlet velocity triangles depending upon speed of the runner defined as low speed runner, medium speed runner and high speed runner.

a. Low speed runner

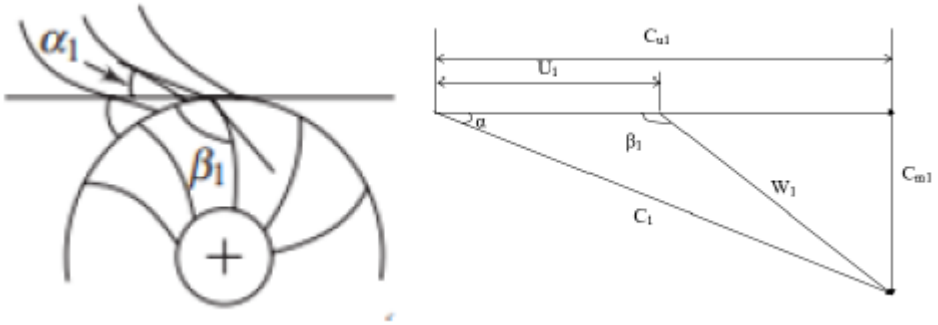


b. Medium speed runner

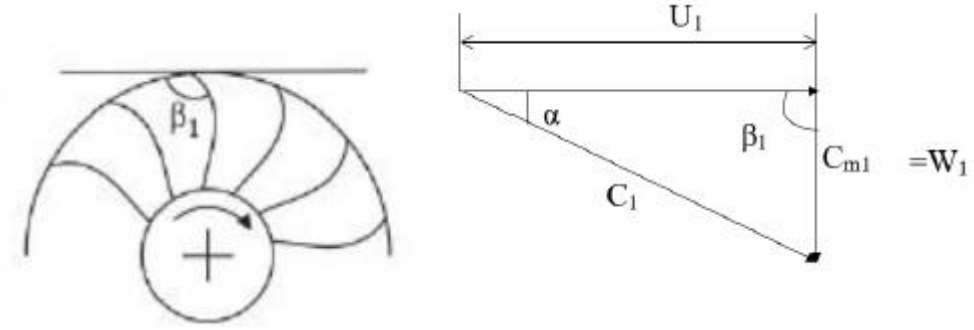


c. High speed runner

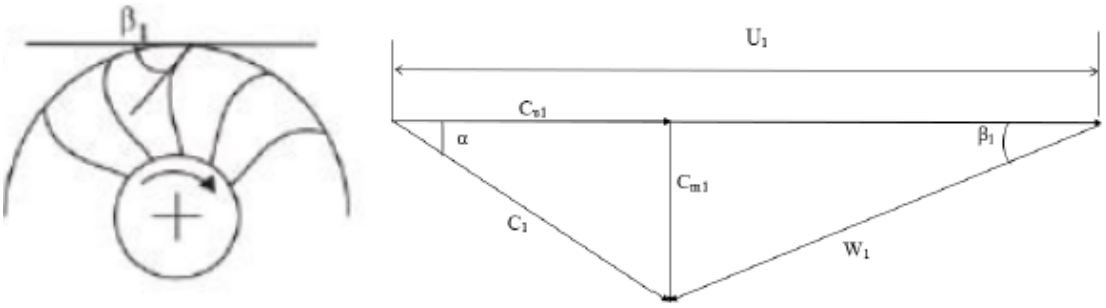


Figure 2.4: Velocity triangles for low(a), medium(b) and high speed(c) Francis runners

When a runner has a low specific speed, their speed is less than their whirl velocity ($U_1 < C_{U1}$). The runner's speed for a medium-specific speed runner is equal to the whirl velocity ($U_1 = C_{U1}$). In a similar vein, a runner with a high specific speed has a speed that exceeds the whirl velocity ($U_1 > C_{U1}$). Figure 2.4 shows the velocity triangles at the intake under various situations.

**2.3 Bovet Method**

There are different methods for designing Francis turbine. Inverse method, direct method, Bovet method are the major method for designing Francis turbine. Among them, Bovet method (Bovet 1963) uses empirical relations to obtain dimensions of Meridional profile of Francis turbine. The method is used for designing of low to medium specific speed hydraulic turbines. This method uses head (H), flow rate (Q), and rotational speed (N) to generate a meridional profile of the blade. The dimensionless specific speed which relates them is calculated using equation.

$$n_o = \frac{N\sqrt{\frac{Q}{\pi}}}{(2gH)^{\frac{3}{4}}}$$

Specific speed $n_o$ is used to calculate the values of runner channel parameters in the meridional plane shown in figure.

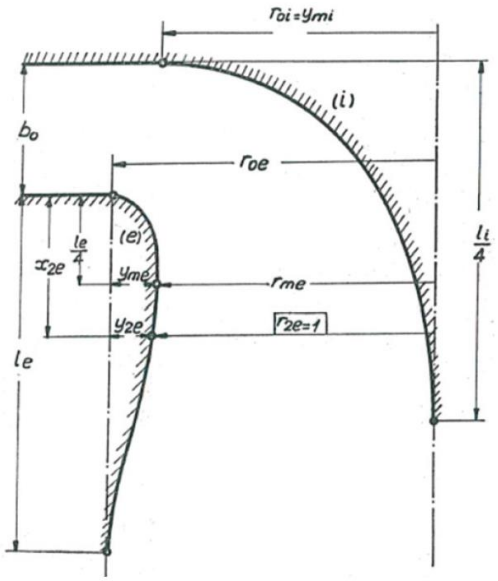


Figure 2.5: Normalized dimensions of the meridional profile

Using the dimensionless specific speed, the dimensions for the flow passages are calculated. The empirical relations are

$$b_o = 0.8(2 - n_o)n_o$$

$$r_{oi} = y_{mi} = 0.7 + \frac{0.16}{n_o + 0.08}$$

$$l_i = 3.2 + 3.2(2 - n_o)n_o$$

$$l_o = 2.4 - 1.9(2 - n_o)n_o$$

$$r_{li} = r_{oe} = \frac{0.493}{(n_o)^{\frac{2}{3}}} \ (n_o < 0.275)$$

$$r_{oe} = 1.255 - 0.3n_o (n_o > 0.275)$$

The above dimensions are normalized so actual dimensions are calculated by multiplying by $R_{2e}$. The relation of $R_{2e}$ is given by

$$R_{2e} = \left( \frac{\frac{Q}{\pi}}{\phi_{2e} N} \right)^{\frac{1}{3}}$$

Where, $\phi_{2e}$ is specific flow which values ranges from 0.26 to 0.28.

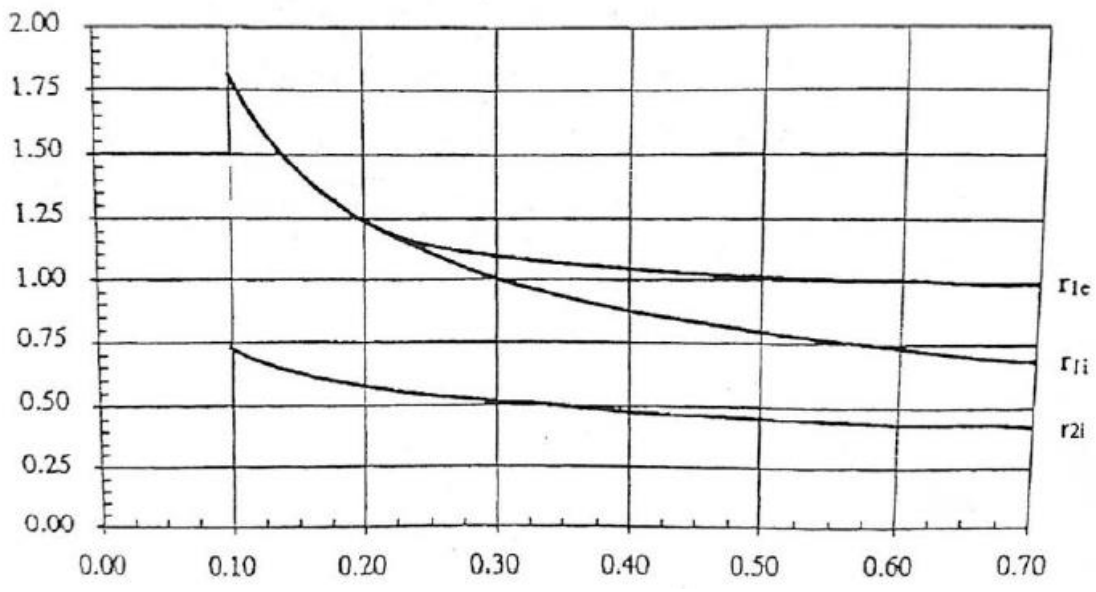


Figure 2.6: Relation between r1e, r1i and r2i with $n_o$ (Radha Krishna 1997)

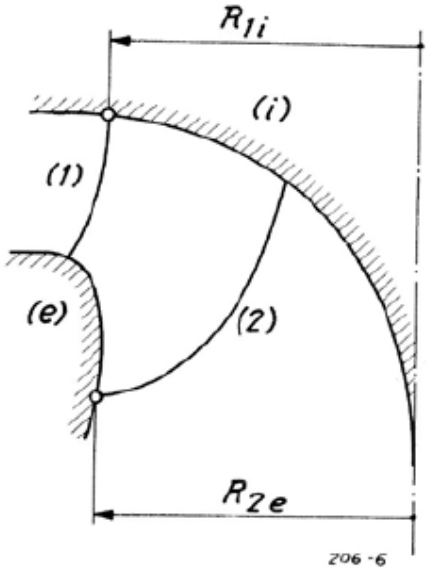


Figure 2.7: Limiting curve of blade

(MILOŞ and BĂRGLĂZAN 2004) employed the Bovet method to determine the meridional profile and the parabola arc method for the leading and trailing edges. The leading and trailing edge curves can be found using the parabola equation. It is stated as

$$y = a(x - h)^2 + k$$

where (x, y) is a point on the parabola and (h, k) is the parabola's center. Point 1e serves as the center and Point 1i serves as a passing point for the leading edge. In a similar

manner, point 2e serves as the trailing edge's center and point 2i serves as its passing point. The hub and shroud curve is given by an equation

$$\left(\frac{y}{y_m}\right)_{i,e} = \left[3.08\left(1-\frac{x}{l}\right)\sqrt{\frac{x}{l}\left(1-\frac{x}{l}\right)}\right]_{i,e}$$

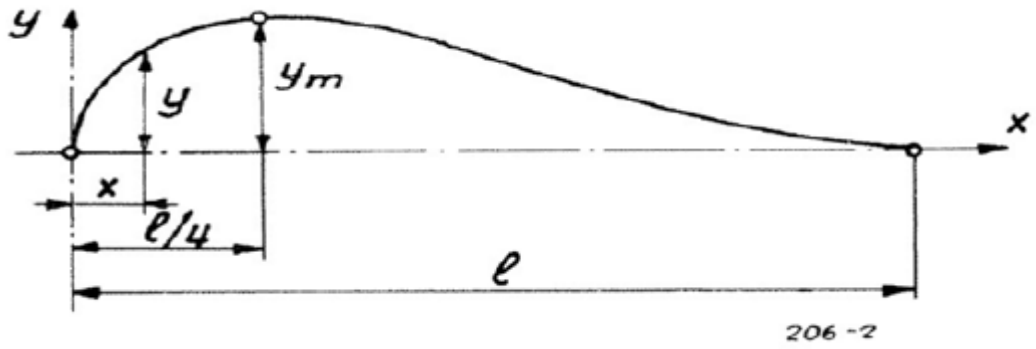


Figure 2.8: Hub and shroud curve of meridional profile

Following figure shows different meridional profiles for different values of $n_o$.

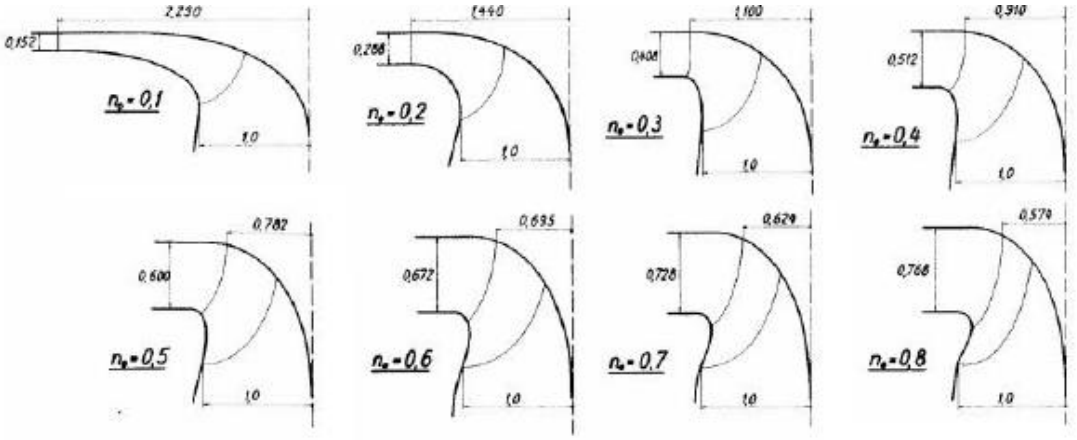


Figure 2.9: Different meridional profiles for different speed number

**2.4 Governing Equation**

The prevalent approach in Computational Fluid Dynamics (CFD) involves solving the discretized form of the Navier-Stokes equations on a grid representation of the geometry, utilizing the finite volume method. The incompressible Navier-Stokes equations, within this context, describe the behavior of fluid flow, accounting for factors such as viscosity and pressure.

$$\frac{\partial u_i}{\partial x_i} = 0$$

$$\frac{\partial u_i}{\partial t} + \frac{\partial u_i u_j}{\partial x_j} = -\frac{1}{\rho}\frac{\partial p}{\partial x_i} + \nu\frac{\partial^2 u_i}{\partial x_j^2}$$

Above equations are the continuity and momentum equation. These equations have the capability to accurately predict pressure and velocity distributions within a specified region. Nonetheless, the computational time required for solving the Navier-Stokes equations on an industrial scale is currently unfeasible with available computers. This challenge arises due to the substantial difference in scale between the overall flow domain and the smallest dissipative scales. These scales can be as small as micrometers or even nanometers, whereas the domain itself may span several meters. Given that achieving a resolution comparable to the dissipative eddies in Direct Numerical Simulation (DNS) is necessary, the domain might demand an immense number of elements—potentially in the trillions—which surpasses current computational capabilities.

### 2.4.1 Turbulence Modeling

Because of the impossibility to solve the Navier-Stokes equations for turbulent flows, numerous attempts have been made to mimic some or all of the turbulent fluctuations using either LES (Large Eddy Simulation) or RANS (Reynolds Averaged Navier-Stokes). RANS models all velocity variations, whereas LES models just scales less than the grid size. RANS equations are written down as

$$\frac{\partial \bar{u}_\iota \bar{u}_\jmath}{\partial x_j} = -\frac{1}{\rho}\frac{\partial \bar{p}}{\partial x_i} + \frac{\partial}{\partial x_j}\left(\frac{\nu \partial \bar{u}_\iota}{\partial x_j} - \overline{u_\iota{}' u_\jmath{}'}\right)$$

The final term, $\overline{u_\iota{}' u_\jmath{}'}$ is referred as the Reynolds stress tensor. This is the term that presents a challenge in the RANS modeling approach because it is unknown and must be modelled. Because the tensor is symmetric, RSM (Reynolds stress modeling) solves one transport equation for each of the tensor components, resulting in six extra equations to solve. The key advantage of this model is that turbulence formation is solved for rather than simulated, which means it is considerably more sensitive to curvature effects, buoyancy, and other anisotropic factors. The issue is that solving these equations is more expensive than solving a two-equation model. A number of approaches, such as the EARSM and the SSG model, have been developed to maintain anisotropy while reducing the processing load of the RSM (Speziale, Sarkar, and Gatski 1991) (Wallin 2000).

The most frequent approach for modeling Reynolds stresses is to employ Boussinesq's assumption, that $\overline{u_i{}'u_j{}'}$ may be approximated with a turbulent viscosity, to add to the laplacian term in the Navier-Stokes equations. According to Boussinesq's assumption, the Reynolds stress tensor is proportional to the trace-less mean strain rate tensor and can be expressed as

$$\overline{u_i{}'u_j{}'} = 2\nu_t S_{ij} - \frac{2}{3}k\delta_{ij} = \nu_t\left(\frac{\partial \overline{u_i}}{\partial x_j} + \frac{\partial \overline{u_j}}{\partial x_i}\right) - \frac{2}{3}k\delta_{ij}$$

In the case of incompressible flow, where $\delta_{ij}$ is the Kronecker delta. The RANS equations with turbulent viscosity approximation are as follows:

$$\frac{\partial \overline{u_i}\overline{u_j}}{\partial x_j} = -\frac{1}{\rho}\frac{\partial \bar{p}}{\partial x_i} + \frac{\partial}{\partial x_j}\left((\nu + \nu_t)\frac{\partial \overline{u_i}}{\partial x_j}\right)$$

The purpose of eddy viscosity based turbulence models is to forecast the value of $\nu_t$ as accurately as feasible. This is a challenging undertaking since turbulence is nearly usually anisotropic, which the scalar $\nu_t$ cannot account for. Since the advent of VR models in recent years, which combine high model resolution accuracy with manageable computational costs, this deficit has been the focus of turbulence modeling research. In order to model the tiny, isotropic scales and resolve the big, anisotropic scales, the velocity field is filtered.

The conventional virtual reality model, known as LES, resolves all scales greater than the grid resolution while modeling scales smaller than the grid size with a sub-grid model. The choice of turbulence model has less of an effect on the solution than a RANS model because only the smallest scales are modeled, and the isotropy assumption also holds truer for small eddies.

The drawback of LES is that it requires the grid resolution and filtering width to be in the inertial sub-range of the turbulent spectrum. While this might not be an issue in the flow's center, the resolution at the walls is extremely fine and frequently precludes the use of LES in most real-world applications.

ILES, or implicit LES, is a technique that is becoming more and more common. Rather than using an explicit sub-grid scale model, the discretization approach is chosen so that the sub-grid model is implicitly replaced by numerical diffusion. This is a practical,

as opposed to theoretical, method to modeling turbulence, emphasizing outcomes above mathematical concepts.

DES, VLES, PANS, and ZLES are a few of the models that have been developed to combine the high accuracy of the LES approach with computing requirements that are more in line with URANS methods. In order to account for the decrease in resolved turbulence, the sub grid viscosity in DES is explicitly raised near the walls. The grid size of VLES is larger than the inertial sub-range scales because it is a coarser simulation of an LES than a true LES. With no specific filtering width used, PANS is produced as a partially resolved, partially modeled technique. Rather, the ratio of simulated scales to all scales is defined using coefficients.

### 2.5 Reviewed Paper

The study by (Elikalfa et al. 2016) outlines the rehabilitation of the Francis turbine runner at the Kepez 1 Hydroelectric Power Plant in Turkey. The project's objectives are to enhance power generation, improve efficiency, and address cavitation issues. Using Computational Fluid Dynamics (CFD), the paper designs a new runner geometry, which, when compared to the existing design, demonstrates significant improvements in cavitation characteristics, efficiency, and power output. This rehabilitation effort promises increased performance for the hydroelectric power plant.

The paper by (Prasad Shrestha et al. 2013) focuses on the optimized design of a Francis turbine runner specifically tailored to operate efficiently in sand-laden water conditions. The study employs computational modeling and simulations to achieve a design that enhances turbine performance and durability, with potential benefits for hydroelectric power plants facing such challenging environments.

The paper by (Khanal et al. 2016) addresses the issue of sediment erosion in hydroelectric turbines, focusing on Francis runner blade design. It aims to determine the optimal outlet angle ($\beta_2$) and blade angle distribution to minimize erosion while maintaining high efficiency. Using simulations and hydrodynamic theory, the study identifies the best blade configuration for given flow rate, head, and sediment flow rate. The optimized blade design is compared to a reference blade, demonstrating reduced erosion and improved efficiency.

(Kocak et al. 2017) involved the design of a Francis turbine runner blade using analytical calculations and numerical simulations. The Bovet approach was utilized to

design a single blade, and Ansys Bladegen V16.1 was employed for blade geometry creation. A fine mesh quality tetrahedron mesh was generated using Ansys Meshing, and the k-ε turbulence model was chosen for steady-state analysis. The numerical results revealed that the Bovet design approach achieved a runner efficiency that differed by only 1% from the committed efficiency. However, negative pressure at the suction side inlet posed the risk of cavitation and oscillation.

The study by (Chen and Choi 2016) highlights the crucial role of the runner in Francis turbine performance. It emphasizes the effectiveness of one-dimensional hydraulic design methods for optimizing runner blade performance. Specifically, the research focuses on the impact of the blade's port area on turbine performance. Findings indicate that the port area significantly influences the outflow angle from the runner passage, with a correctly designed exit flow angle reducing energy loss in the draft tube, ultimately improving turbine efficiency.

This paper by (MUNTEAN Sebastian, Romeo F. SUSAN-RESIGA, Sandor BERNAD 2004) conducts a numerical investigation of 3D flow within the distributor (comprising stay vanes and guide vanes) of the GAMM Francis turbine. The computational domain encompasses the interblade channel of the distributor and includes upstream and downstream boundaries represented by cylindrical and conical patches, respectively. Inlet conditions assume an ideal spiral casing with constant radial and circumferential velocity components and zero axial velocity. The outlet section considers a measured pressure profile. The study addresses three main aspects: computing distributor flow for various guide vane angles to derive guide vane torque versus opening angle, exploring flow patterns for the entire range of guide vane positions at different locations of the guide vane axis.

The paper by (Kaniecki and Krzemianowski 2016) discusses Computational Fluid Dynamics (CFD) calculations conducted on a model test turbine with two different runners, designed by ZRE and IFFM. The focus was on replicating the test rig geometry to model future test conditions accurately. CFD simulations covered a wide range of rotational speeds, primarily through steady calculations, with future plans for transient calculations. The results indicated that the ZRE model turbine achieved a hydraulic efficiency of 92.3%, while the IFFM design reached 90.0%. Both designs attained high design-specific speeds (98 and 114), aligning with project goals. Based on CFD results,

the ZRE runner was chosen for manufacturing and further laboratory testing, with final verification planned during model tests at the IFFM test stand.

In study by (Aradag, Akin, and Celebioglu 2017), a 4.3 MW Francis turbine was meticulously designed using computational fluid dynamics (CFD). Each component of the turbine underwent separate CFD analysis, and a comprehensive analysis was conducted to confirm the overall design's efficiency. CFD simulations were extended to off-design conditions, ensuring the turbine's high efficiency across a wide range of flow rate-head combinations. The research demonstrates that "part by part" CFD simulations, where each turbine component is designed separately, align well with "full turbine" simulations, which require significant computational resources. The designed turbine achieved an efficiency of 90-92% across a broad range of head and flow rate values, making it adaptable to seasonal variations in operating conditions. Ultimately, this efficient turbine design was implemented in an actual power plant.

The study by (U. Shrestha, Chen, and Choi 2019) considered various sediment parameters to identify correlations and vulnerable runner locations. It depicts erosion rates at different spans, highlighting spans 3 and 4 near the runner's shroud as highly affected areas. The research shows that erosion is most pronounced near the trailing edge of the runner, particularly in stream 3. In conclusion, the trailing edge and shroud region are the most susceptible to erosion in Francis turbines, especially in high specific speed turbines where acceleration erosion prevails. Sediment concentration has a direct relationship with erosion rate density, while the relationships between sediment size, shape, velocity, and erosion rate density are less predictable. Among these factors, sediment shape factor and concentration exert the most influence on erosion rate density within the runner.

CFD analysis by (Baidar et al. 2015) of a high head Francis turbine for the Tara Khola micro hydro project in Nepal aimed to determine the optimal number of blades. Among the options tested (11, 13, and 17 blades), the 13-blade configuration offered the best balance of efficiency, variable discharge performance, and manufacturability. However, it came with a higher risk of sediment erosion compared to the 17-blade runner.

This study by (Kaewnai and Wongwises 2011)aims to enhance the design of a Francis turbine runner and assess its performance using Computational Fluid Dynamics (CFD).

The design process involves calculating various dimensions and parameters for the runner under specific conditions. CFD simulations were conducted, revealing that the head rise at the design point fell short of the specified head. To address this, modifications were made to the meridional plane and blade angles. Through these adjustments, the head rise approached the specified value, and the overall runner performance reached approximately 90% at the design point. The study suggests that this method can effectively simulate Francis turbine runner performance.

## CHAPTER 3: RESEARCH METHODOLOGY

In this research, optimization of the Francis turbine designed using Bovet method is done. Optimization is done in two steps. First is size optimization and the second is shape optimization of meridional profile generated using Bovet method.

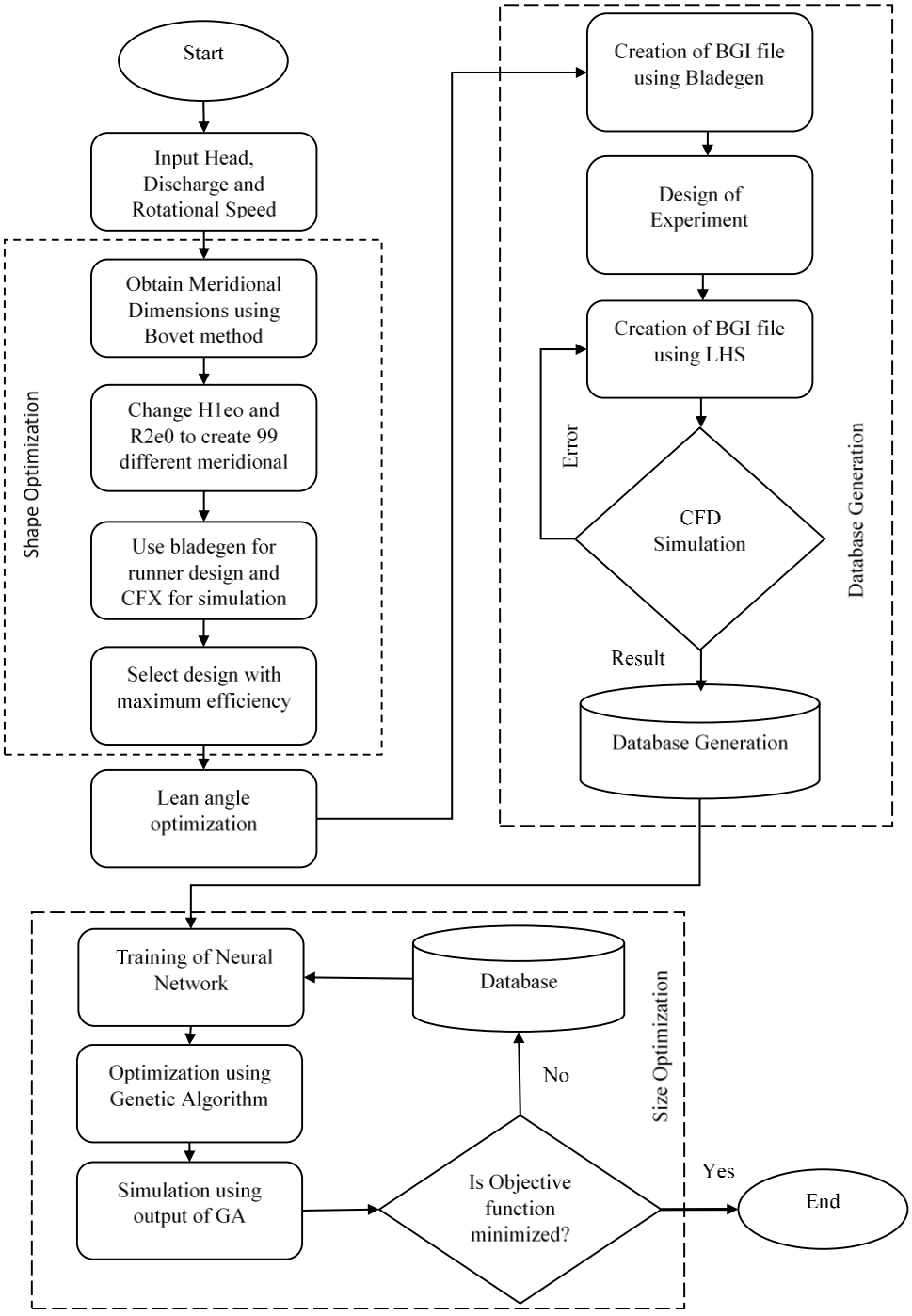


Figure 3.1: Methodology of research

The research is divided into three segment: Size Optimization, Database Generation, Shape Optimization and finally manufacturing and testing.

### 3.1 Input Parameters

Head, flow rate and rotational speed are the input parameters for designing of Francis turbine using Bovet method. The method provides dimensions of meridional profiles which further is imported to bladengen, Ansys and final design is generated. Table 3.1 gives the input parameters of designed turbine.

Table 3.1: Input parameters for turbine design

| S.N. | Input Parameters | Values | Units |
|---|---|---|---|
| 1. | Head | 15 | m |
| 2. | Flow rates | 0.12 | $m^3/s$ |
| 3. | Rotational speed | 1500 | RPM |
| 4. | Vane thickness factor | 0.96 | |

### 3.2 Size Optimization

This research was divided into three categories. Size optimization, shape optimization and finally manufacturing and testing. Two variables Hlio and V2e0 changes the size of the runner which can be changed from 0.2-0.3 and 1.6-2 respectively. In his paper Bovet also recommended to find the best values of Hlio and V2eo through iteration.

Matlab code was written to design a meridional profile as per Bovet method and it was used to generate the data points of hub, shroud, leading edge and trailing edge. The data points were imported to the bladegen, Ansys to obtain three dimensional runner. Table below shows the different dimensions obtained from the Bovet method.

### 3.3 Numerical Solution

After generating 99 different meridional profiles, they were imported to the bladegen Ansys and complete three dimensional model was generated. For three dimensional runner beta angle at leading edge and trailing edge, blade thickness were given to

bladegen. Linear blade angle distribution was given while lean angle was zero for all the designs.

Ansys TurboGrid relies on a configuration file called BladeGen.inf to establish critical parameters like the rotation axis, blade count, and a unit of length that defines the machine's size. Additionally, this file is essential for identifying curve files, which are subsequently imported to describe the curvature of the hub, shroud, and an individual blade. The software processes the geometric information contained in these input files to create a visual representation, and you can see a rough outline of this representation in the viewer. The generated geometry was imported to TurboGrid Ansys for meshing.

For consuming less computational resources and to reduce the time, efforts and complexity of meshing periodicity of the impeller geometry is taken advantage. The periodic generic sector can be chosen in two different ways. First being the flow passage between two blades (suction side of first blade to pressure side of next blade) and second being one complete blade inside the periodic flow passage. Second method was used in this analysis.  Figure 3.2 shows meshing on a passage using TurboGrid.

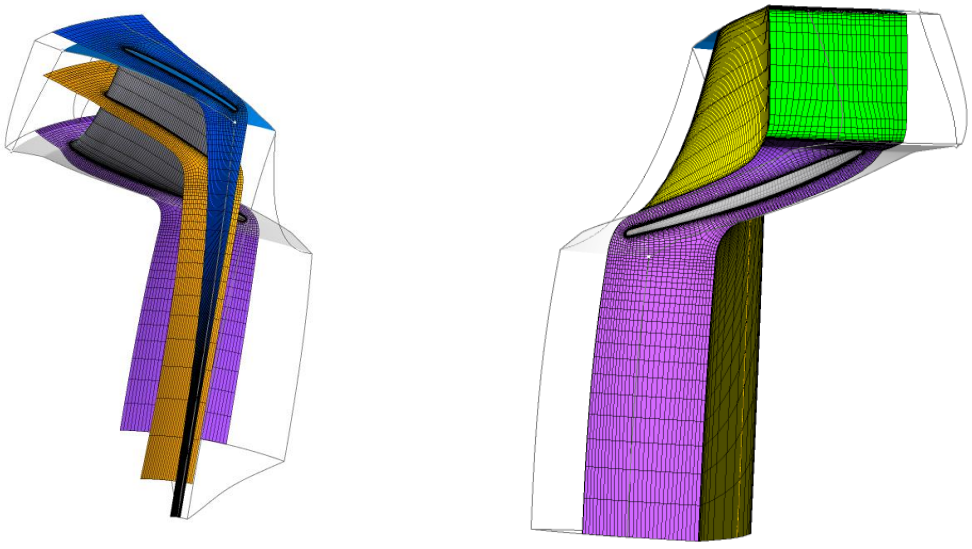

Figure 3.2: Mesh generated in single passage of runner

As batch run was conducted automatic meshing was used. Mesh Below table 3.2 shows mesh parameters that were used for generating mesh.

Table 3.2: Mesh statistics

| **Mesh measure** | **Value** | **%Bad** | **Acceptable limit** |
|---|---|---|---|
| Minimum face angle | 30.26$^{o}$ | 0 % | 15$^{o}$ |
| Maximum face angle | 150.4$^{o}$ | 0 % | 165$^{o}$ |
| Maximum element volume ratio | 6.56 | 0 % | 20 |
| Minimum volume | 6.8x10$^{-13}$ m$^{3}$ | 0 % | 0 |
| Maximum edge length ratio | 378.4 | 0 % | 100 |
| Maximum connectivity number | 10 | 0 % | 12 |

Mesh size, or mesh count, represents the total quantity of cells utilized to occupy the entire flow domain. The appropriate mesh size is determined by the intricacy of the geometric elements and the simulation's intended objectives. It is essential that the number of nodes or cells allocated is adequate for two main purposes: To accurately represent and resolve the intricacies of the geometry and to effectively capture and simulate the underlying flow physics. Mesh independence test was done in order to minimize error associated with lesser number of mesh. Figure 3.3 shows the mesh independence test.

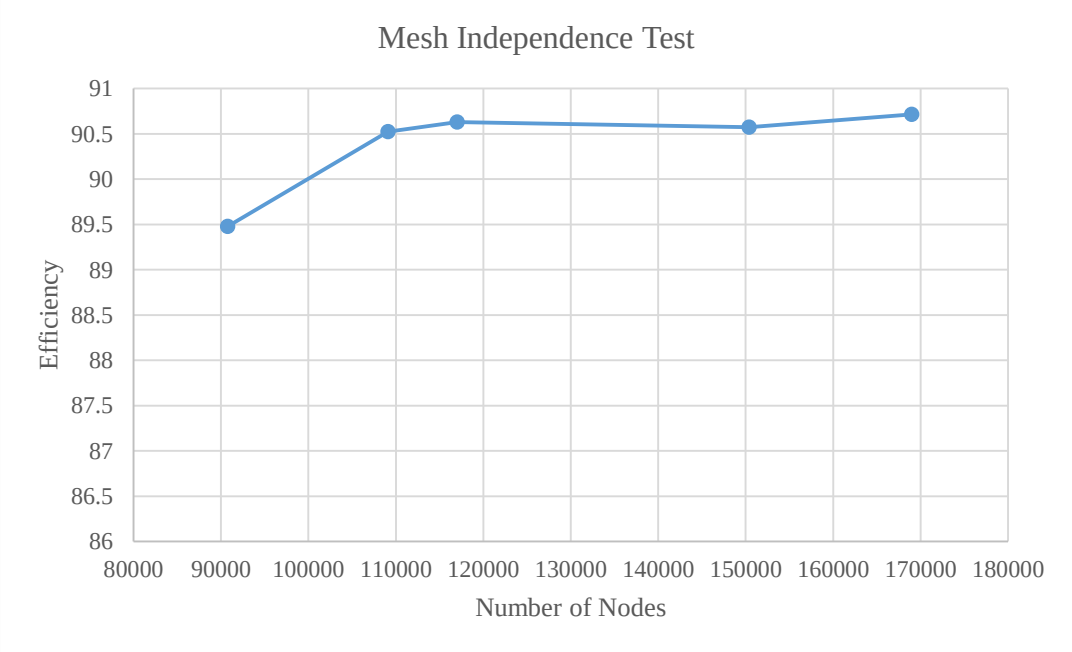


Figure 3.3: Mesh independence test

Table 3.3: Boundary conditions for numerical simulation

| **Boundary Conditions** | |
|---|---|
| Type | Steady State |
| Inlet | Mass flow rate: 119.7 kg/s |
| Flow Direction | Cylindrical components<br>Axial Direction: 0<br>Radial Direction: -0.327<br>Theta Direction: -0.945 |
| Outlet | Static Pressure: 0 atm<br>Reference pressure: 1 atm |
| Hub, Shroud, Blade | No-slip condition |

### 3.4 Lean Angle

The stacking condition dictates the angle of blade lean, denoted as θ, at the entrance edge of the turbine runner blades. This angle is crucial in determining the wrap angle of the blades.

In Figure 3.5, it is evident that the blades are inclined counter to the direction of the runner's rotation. In other words, the blade at the shroud leads the blades at the hub, resulting in a negative θ value. This negative blade lean has a significant impact on the pressure distribution within the runner. Specifically, it amplifies the pressure loading at the hub while reducing the pressure loading at the shroud.

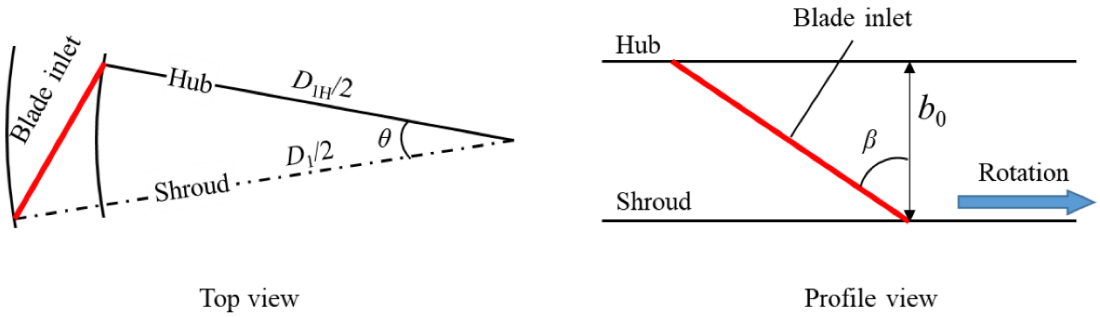


Figure 3.4: Lean angle definition

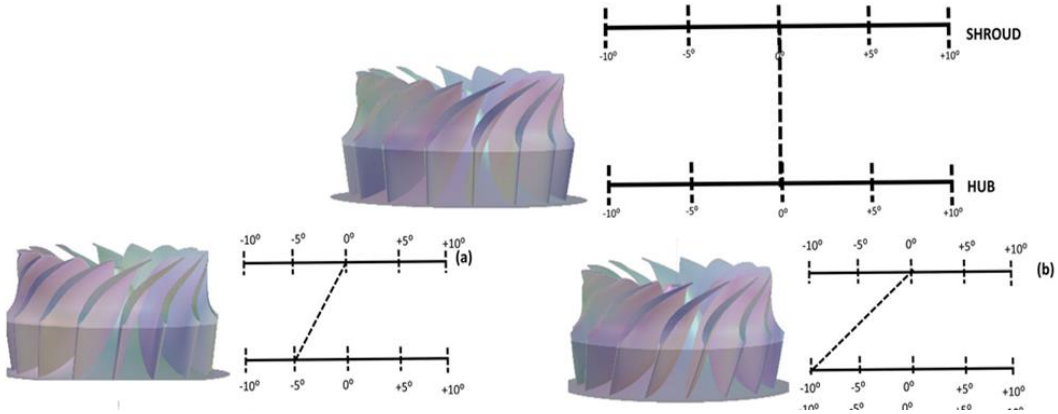


Figure 3.5: Change in shape of leading edge due to change in lean angle

Lean angle was varied from -10 to 10 degree and simulation was conducted.

### 3.5 Latin Hypercube Sampling

Latin hypercube sampling (LHS) is a statistical method for generating a near-random sample of parameter values from a multidimensional distribution. It has several advantages over simple random sampling, such as reducing the sample size needed and ensuring a better representation of the underlying distribution. LHS partitions the range of each parameter into equally probable intervals, ensuring that every interval contains exactly one sample. This clever arrangement, following the Latin square principle, allows for a more even and representative coverage of the entire parameter space, reducing bias in the sampled selections.

The Latin hypercube sampling (LHS) method serves as a sampling strategy designed to achieve uniformity across the entire design space as well as along projected axes. It maintains this uniformity regardless of the number of points generated, making it a versatile choice. Compared to grid-based methods, LHS excels in filling space more effectively, which is why it's favored within the current optimization framework.

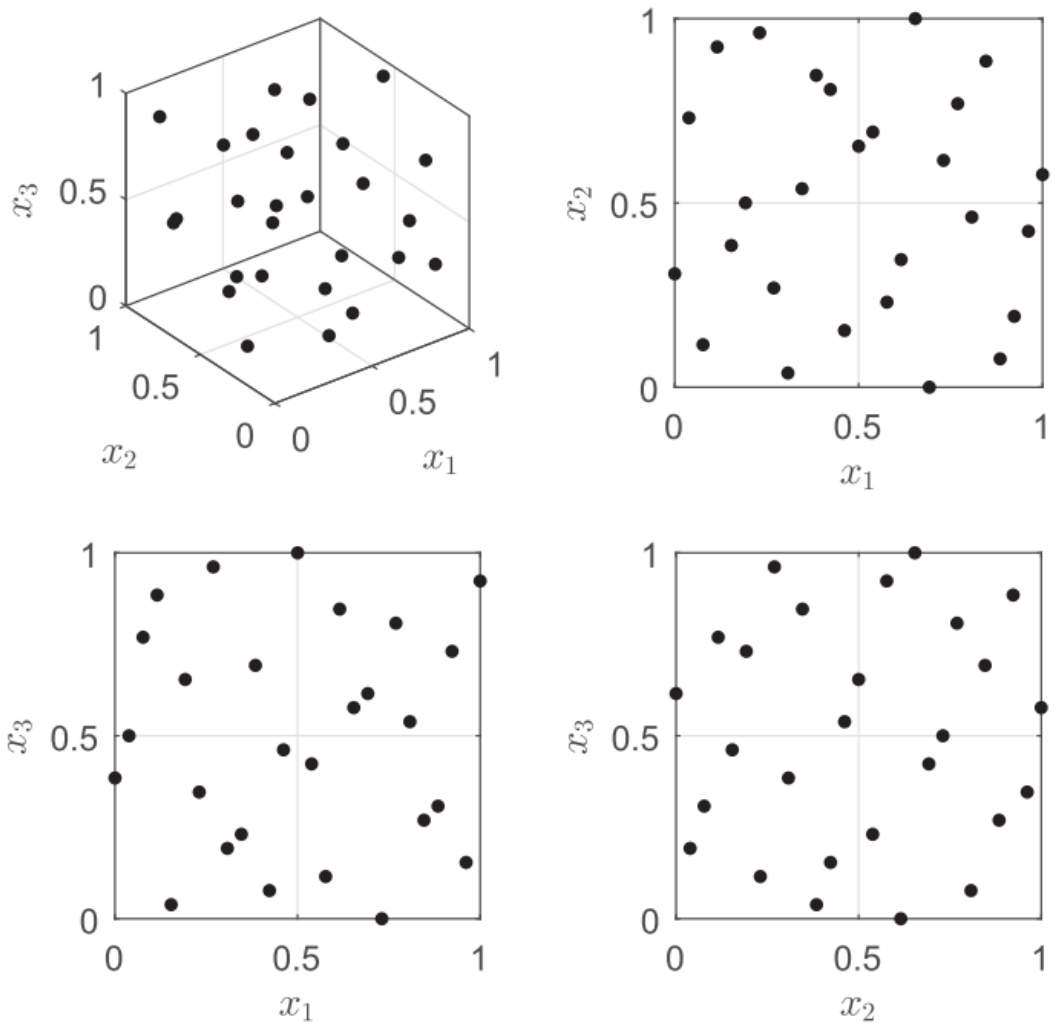


Figure 3.6: Illustration of three dimensions of LHS technique using 27 points for three-variable problem.(Forrester, Sobester, and Keane 2008)

### 3.6 Design of Experiment

In this optimization shape of meridional profile obtained after lean angle optimization was used to generate multiple design samples. For varying the shape of the meridional profile, leading edge, trailing edge, hub, shroud and beta angle distribution curve was varied using Bezier curve. First all the five curves were converted into Bezier curve with four control points. Then two middle control points were varied to obtain multiple samples. Latin Hypercube Sampling (LHS) method was used to generate design samples. With two control points of each curve total ten control points were varied and total of 600 design samples were generated. Figure 3.7 shows the how four curves of meridional curves were varied and figure 3.9 shows the variation created on beta angle distribution curve.

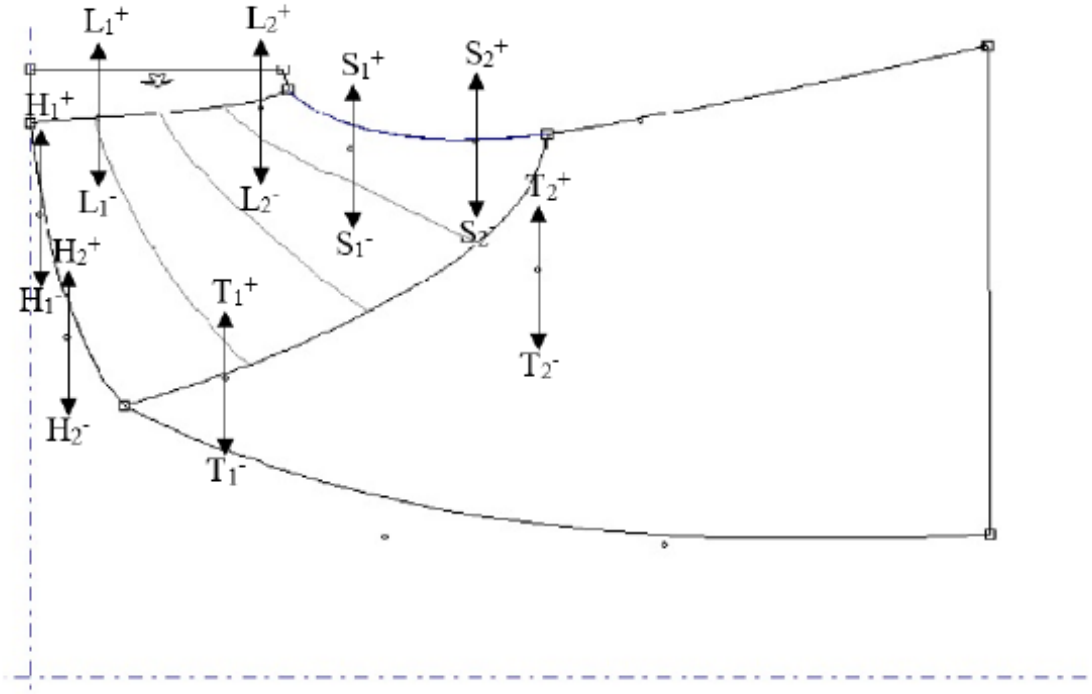


Figure 3.7: Variation of control points in radial direction (Satyal et al. 2022)

In the figure 3.7 T, H, L, and S represents the control points of trailing edge, hub, leading edge and shroud respectively. Out of four control points of each curve only middle two control points were used to change the shape of the meridional profile. Each control points were limited to shift ±10% in radial direction only i.e. vertical direction. Each points were constrained in order to make the process less complicated. Figure 3.8 shows meridional profile of six different design sample including the initial design. With the ability to vary two control points shape of each curve was able to vary in concave, convex and sinusoidal pattern.

Total of 600 design samples were generated and CFD simulation of each design points were conducted. Out of which only 578 design samples simulation were conducted successfully. Major errors occurred during the simulation was due to inability to create mesh in complicated design given by LHS sampling.

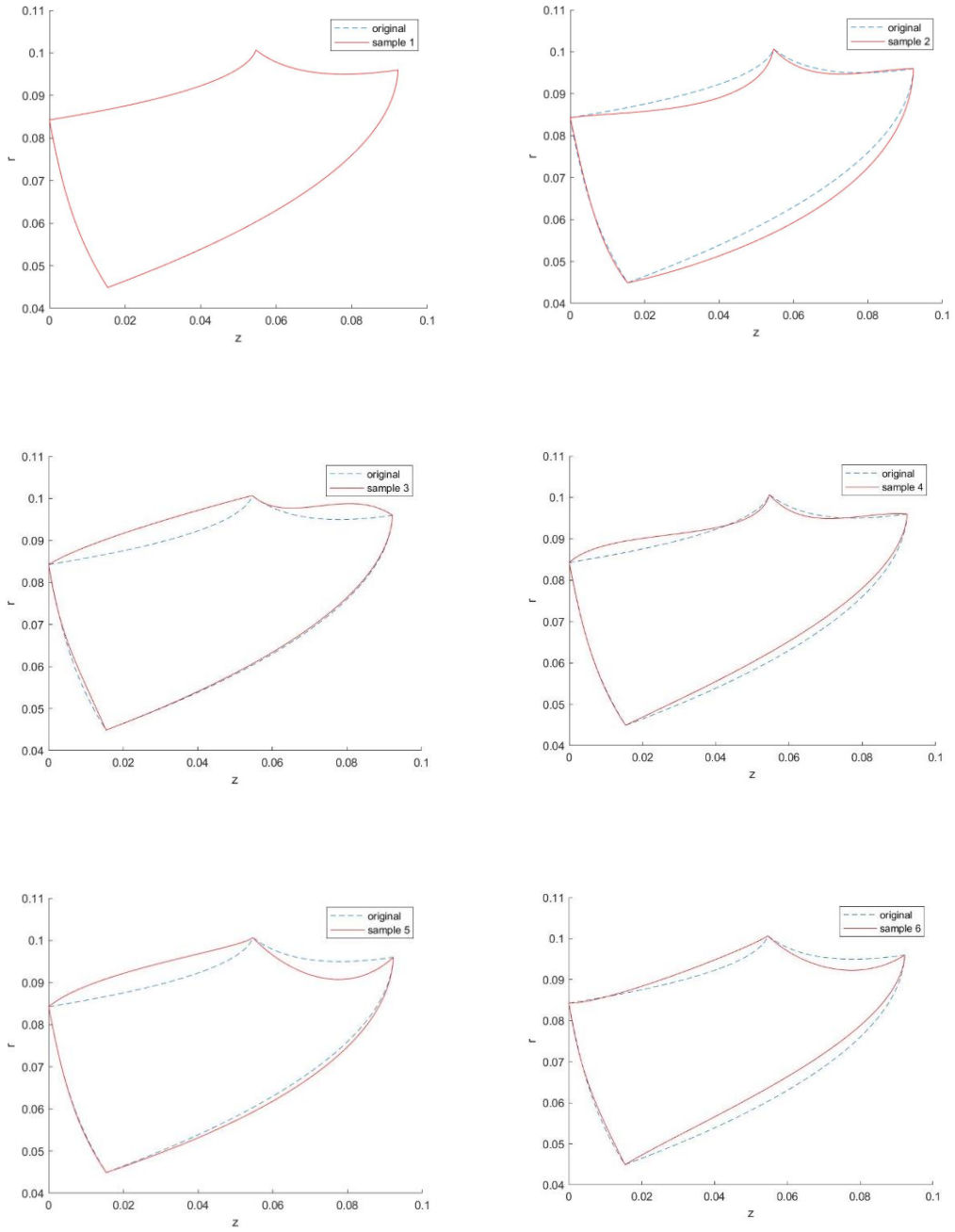


Figure 3.8: Design samples of meridional drawings with different shapes

Figure 3.8 shows six different design points. First sample showing the initial design obtained after shape optimization and lean angle optimization. Other five samples shows the shape variation of meridional profiles.

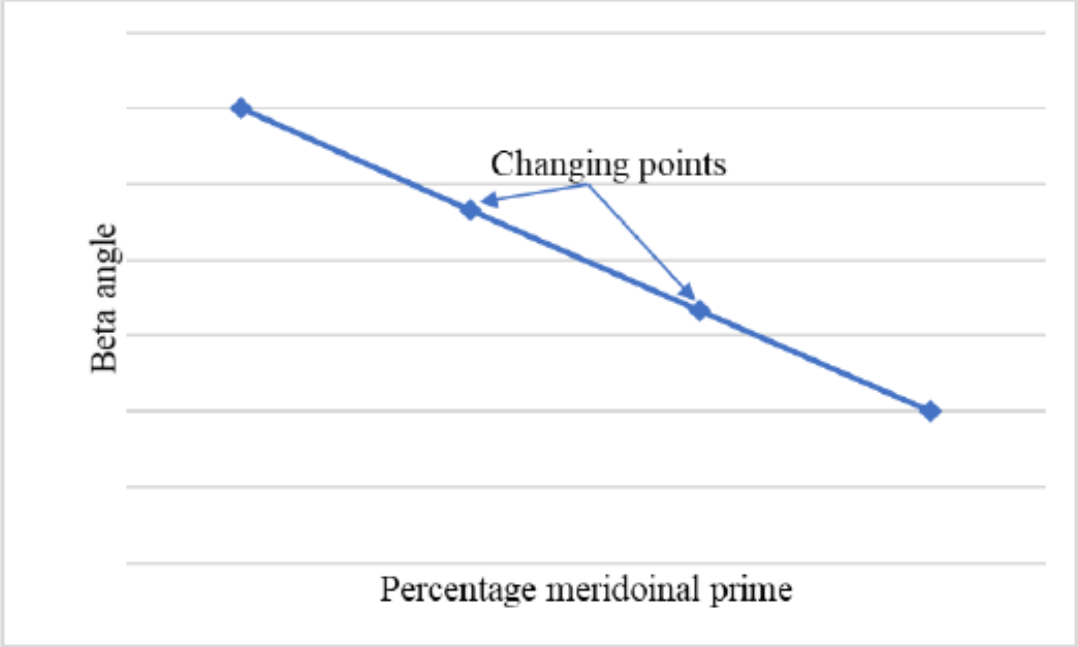


Figure 3.9: Beta angle distribution variation

Also, beta angle distribution from leading edge to trailing edge was varied. It was performed using same technique i.e. using Bezier curve. Figure 3.9 shows how a linear beta angle distribution was converted to Bezier curve using four control points and midpoint two control points were used to change the shape of the distribution. Here also concave, convex and sinusoidal shapes were generated. Figure 3.10 shows six different samples of beta angle distribution containing linear distribution for initial design and other five generated samples.

For analysis blade was divided into five streamlines so, beta angle distribution on five streamlines were generated. Each stream lines were changed similarly to make the optimization process less complicated. Variation of beta angle distribution on each streamlines would have required more number of design samples making the optimization task more laborious and computationally expensive. Control points on Bezier curve were able to shift ±30% in radial direction.

Using this method size optimized meridional profile had been able to change shape and change beta angle distribution. Allowing us to get multiple design points which was further simulated and obtained results from the simulation was used further to train neural network and optimize design using genetic algorithm.

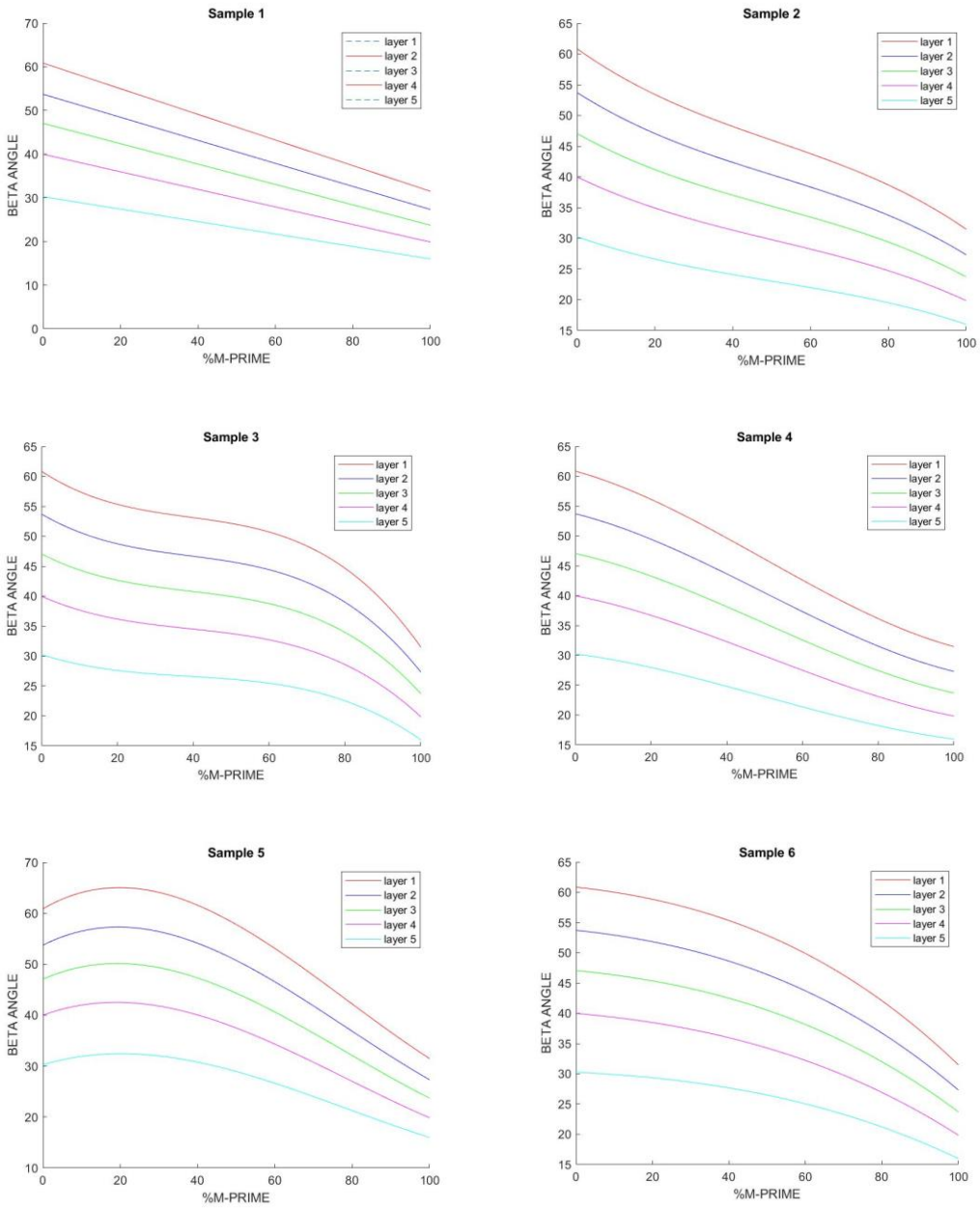


Figure 3.10: Design samples showing different beta angle distribution

### 3.7 Database Generation

After successfully generating 600 design points they were simulated in ANSYS using batch mode. The design generated was imported to ANSYS BladeGen and then transferred to TurboGrid for meshing. As design samples was larger individual control of mesh wasn't possible so automatic meshing using Adaptive Tetrahedral Meshing (ATM) was done. Regarding the number of mesh, mesh independent test was performed in initial design and using the similar setup meshing on all the design sample was conducted.

ANSYS CFX was used for simulation. Results obtained were methodically logged and kept together with their respective design points to create the database.

### 3.8 Neural Network

A neural network model with a multi-layer perceptron structure was trained using the initial database in order to produce a response surface. Four layers were included in this model: an output layer, two hidden levels, and an input layer. Input layers contains ten neurons while output layer contains only one neuron. The output layer used a linear activation function, whereas the hidden layers used the Rectified Linear Unit (ReLU) activation function, per research and previous studies' recommendations. Trial and error was used to determine the number of neurons, and eight neurons were chosen for the second layer and four neurons for the third layer. Output generated from the simulation was used to train this neural network.

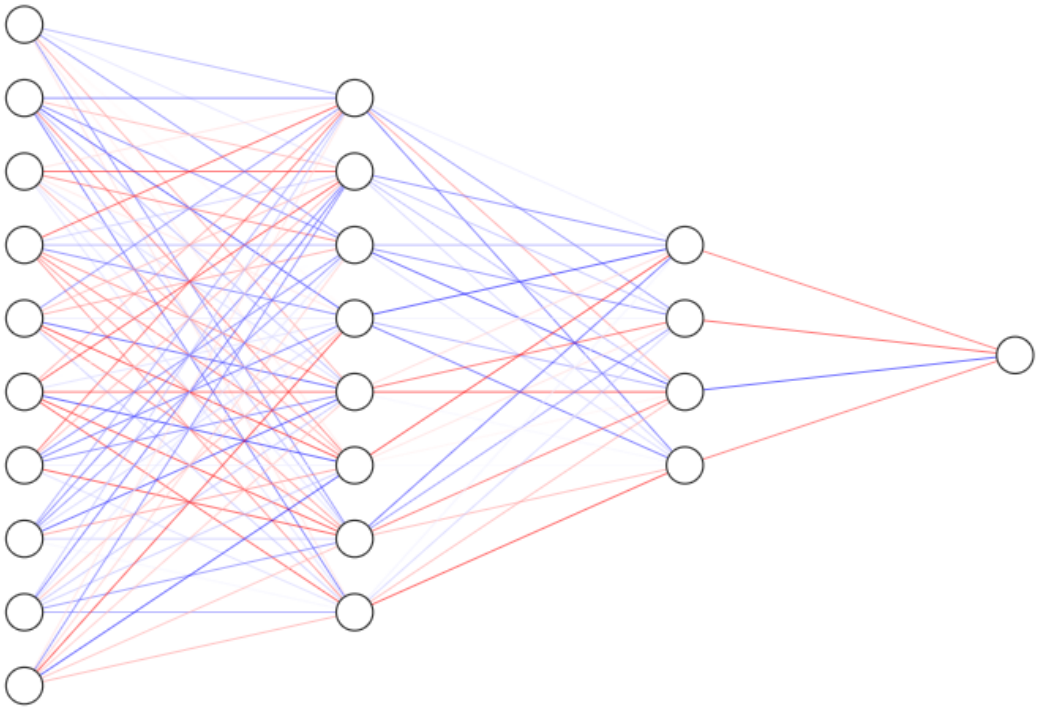

Figure 3.11: Neural Network

### 3.9 Genetic Algorithm

Genetic algorithm was used as the optimization function using the objective function. Specifications of genetic algorithm was set as per the previous study conducted by (Satyal et al. 2022) which is given below.

Table 3.4: Specifications of Genetic Algorithm

| | | | |
|---|---|---|---|
| Population Size | 300 | Crossover function | Crossoverscattered |
| Generations | 150 | Crossover fraction | 0.8 |
| Fitness scaling function | Fitscalingrank | Crossover count | 228 |
| Selection function | Selectiontochunif | Mutation function | Mutationgaussian |
| Elite count | 15 (5%) | Mutation count | 57 |

The functioning of a Genetic Algorithm (GA) in the optimization process is depicted in Figure 3.20. It illustrates how a neural network is connected with the stages of selection, crossover, and mutation to calculate the fitness value. A population of 300 candidates was used in each of the 150 iterations of the GA.

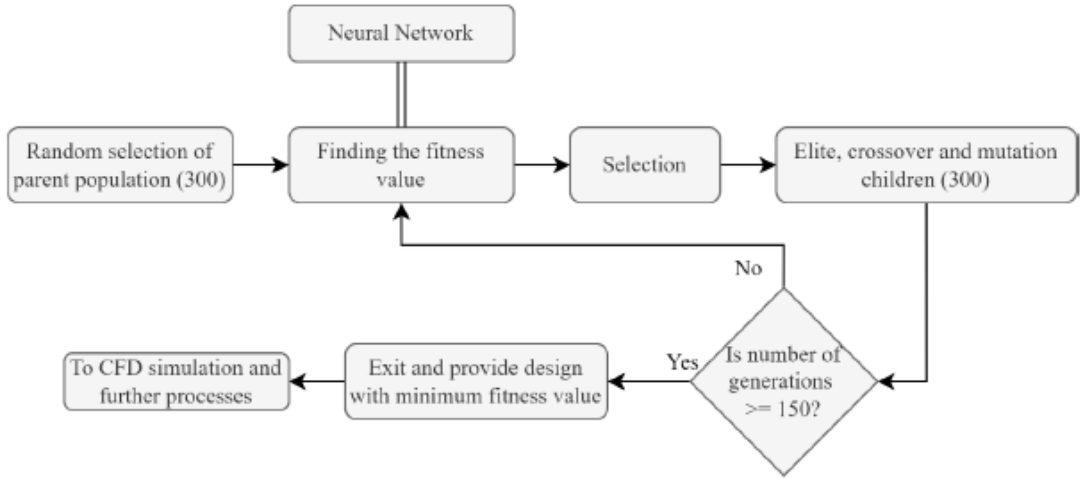


Figure 3.12: Flowchart of GA, ANN and CFD conjunction (Satyal et al. 2022)

The GA was intended to work in tandem with the neural network's response surface to determine which runner candidate is best. The candidate was then simulated, and the value of its objective function was determined. The neural network was then retrained using this revised dataset when the data related to this candidate was added back into the database. To improve the optimization, this procedure was carried out again.

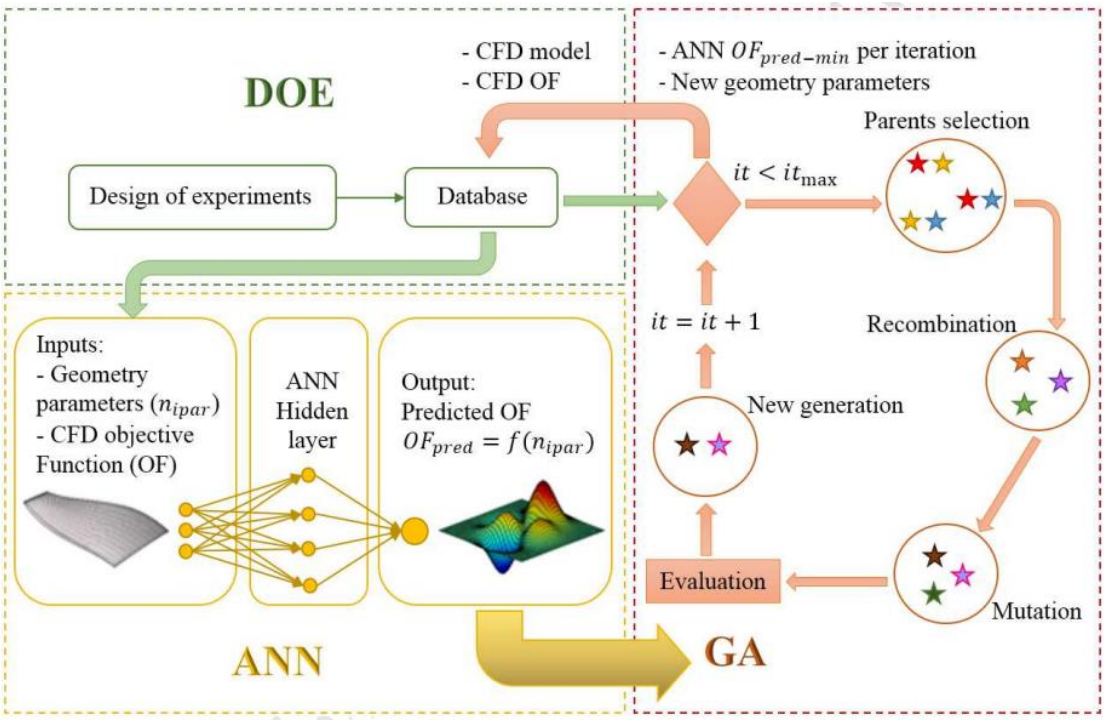


Figure 3.13: Schematic process of the integrated DOE-ANN-GA optimization.(Aponte et al. 2020)

### 3.10 Objective Function and Optimization

It is crucial to design a hydraulic turbine to satisfy particular performance standards. Engineers set up an objective function and constraints that take into account various design elements in order to accomplish this. In a particular situation, the parameter we want to minimize or maximize is represented by the objective function.

The goal of (Aponte et al. 2020) and (Teran, Larrahondo, and Rodr\'\iguez 2016) study was to minimize the objective function value, which was determined by adding up the penalties related to each parameter. Each penalty term was then given a weight factor to represent the relative importance of each variable during the optimization process.

$$OF = w_\eta \left(\frac{\eta_{req} - \eta}{\eta_{req}}\right)^2 + w_h \left(\frac{H_t - E_t}{H_t}\right)^2 + w_e \left(\frac{ErT_{new\ design}}{ErT_{reference\ design}}\right)^2 + w_c \left(\frac{A_{req} - A}{A_{req}}\right)^2$$

There are four components in the objective function. The efficiency penalty is expressed by the first term, where $\eta$ is the efficiency of the planned runner and $\eta_{req}$ is the required runner efficiency, which is 100%. The second element is the head penalty; in our optimization issue, the needed head is 15 meters, and $H$ is the head of the

designed runner. The erosion factor, which functions as an erosion penalty based on suggestions from the literature, is the third term. The reference design's erosion propensity is identified at 124.4 $m^3 s^{-3}$. In a similar vein, cavitation is penalized in the fourth term, which is quantified by the cavitation surface area of the intended runner ($A$) and the necessary surface area for cavitation ($Areq$). The prescribed surface area for cavitation is an extremely small value of 2.2E-05 $m2$.

The weights given to each penalty term are represented by the variables $w\eta$, $wH$, $we$, and $wc$ in this objective function. The values of these weights are 45, 10, 0.1, and 6E-05, in that order. These weight values are calculated so that the average value of each penalty phrase is one. Furthermore, in order to severely penalize departures from the required head, more weight is assigned to the head penalty term; in a similar vein, the efficiency penalty term receives more weight based on conversations with supervisors.

# CHAPTER 4: RESULTS AND DISCUSSION

## 4.1 Design Variation

For the size optimization ninety-nine different size design of meridional profile were generated. They were imported to Ansys bladegen to obtain runners. Turbogrid was used for meshing the runner. Then Ansys CFX was used for simulation. For size optimization efficiency was the only variable. Following figures shows the minimum and maximum size of the runner obtained.

## 4.2 Parametric Size Optimization

Parametric optimization for size was carried out by varying two variables from Bovet method which changes inlet diameter and outlet diameter of Francis turbine. Total of ninety nine runner design of varying size were generated and simulation was performed. Optimized design was obtained by selecting the size of runner of maximum efficiency. Table 4.1 and figure 4.1shows the size variation of largest runner and smallest runner.

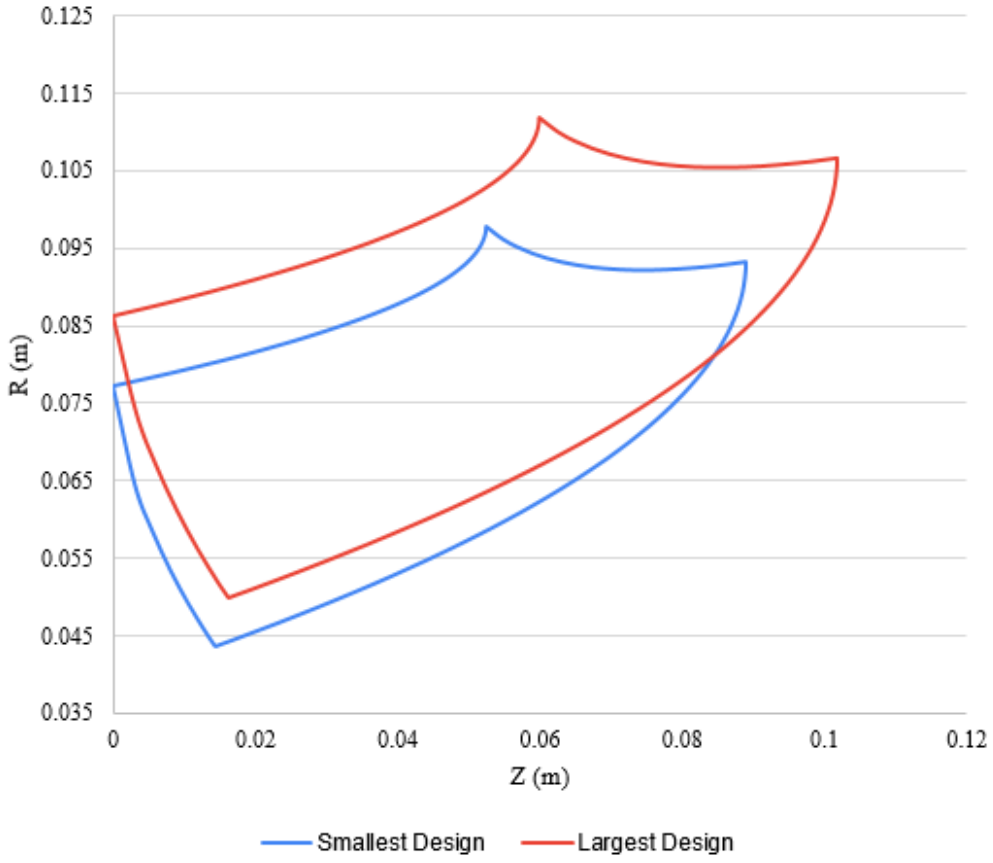


Figure 4.1: Size of smallest and largest runner used in size optimization

Table 4.1: Dimensions of largest and smallest runner

| Dimensions | Largest Runner | Smallest Runner | Optimized Runner |
|---|---|---|---|
| $B_o$ | 5.78 cm | 5.05 cm | 5.17 cm |
| $R_{2e}$ | 10.67 cm | 9.32 cm | 9.54 cm |
| $R_{li}$ | 8.63 cm | 7.72 cm | 8.43 cm |
| $L_e$ | 11.88 cm | 10.38 cm | 10.62 cm |

In the above table 4.1 shown the major dimensions of largest runner, smallest runner and optimized runner. In comparison to the smallest runner, largest runner inlet is 14% larger and optimized runner is 2.4% larger. $R_{li}$ also known as inlet diameter, largest runner is 11.8% and dimension of optimized runner is 9.2% larger than the smallest design.

The surface plot shown in figure 4.2 shows the efficiency of different runners according to size i.e. varying h1i0 and r2e0.

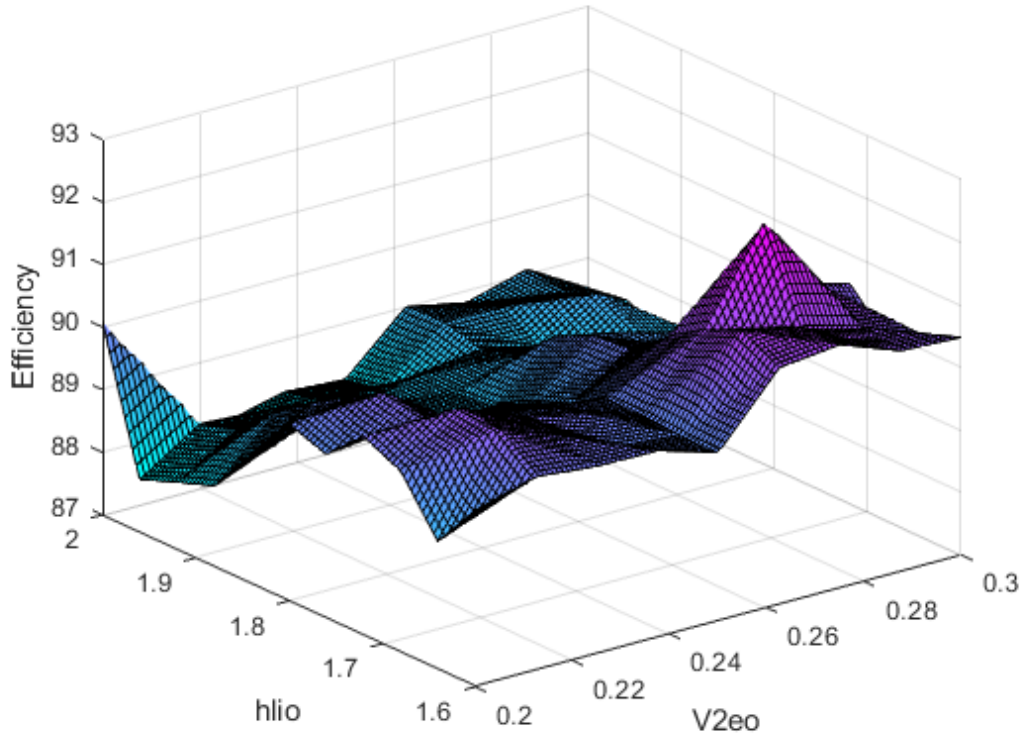


Figure 4.2: Size optimization of runner

The maximum efficiency was found to be 92.3% for corresponding hlio and V2eo values of 1.68 and 0.28 also minimum efficiency was found to be 87.84% for corresponding hlio and V2eo values of 1.68 and 0.28. The surface plot indicates that the maximum efficiency lies around higher values of V2eo and lower values of hlio.

Following figures contains more detailed information regarding simulation results of optimized runner.

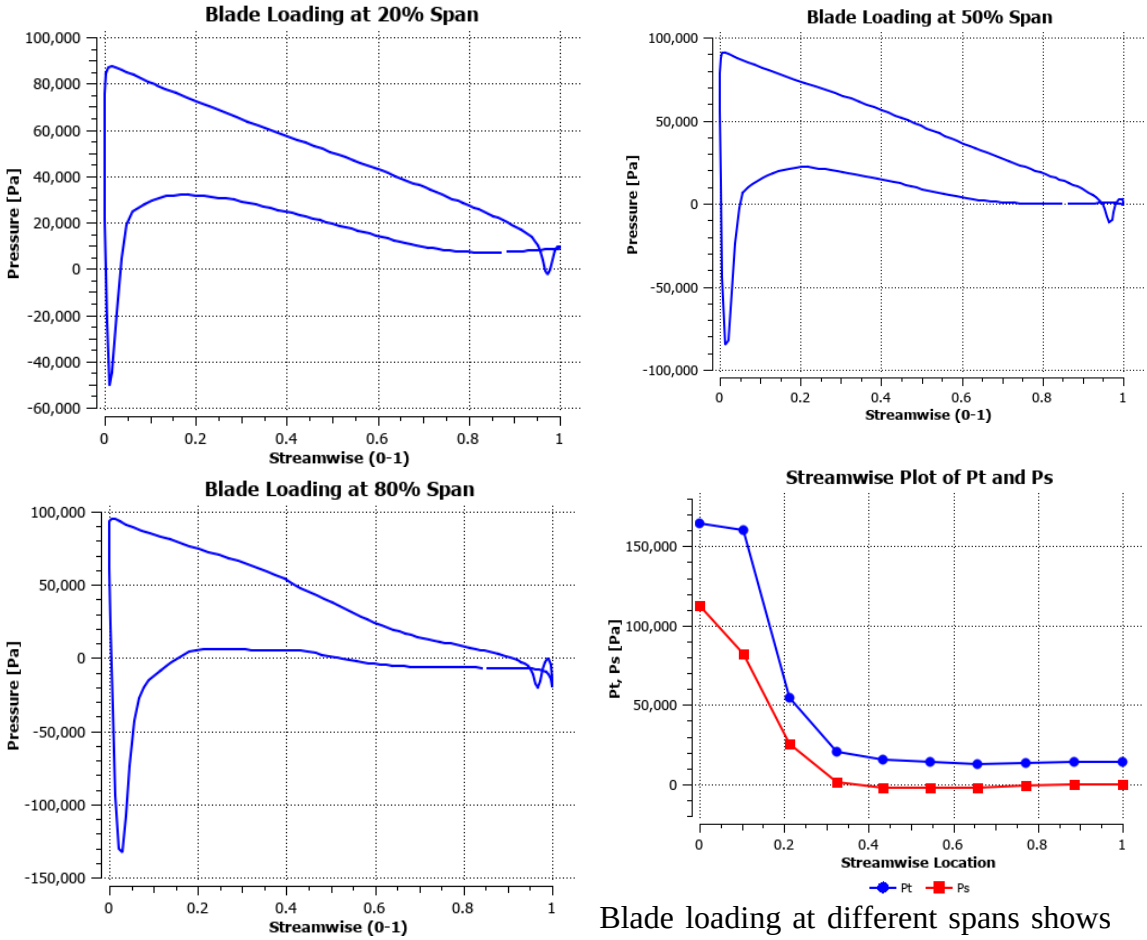


Figure 4.3: Blade loading at 20%, 50% and 80% span and stream wise plot of total pressure and static pressure

Blade loading at different spans shows pressure variation in suction and pressure side of runner. It also indicates the work extraction from different section of blade.

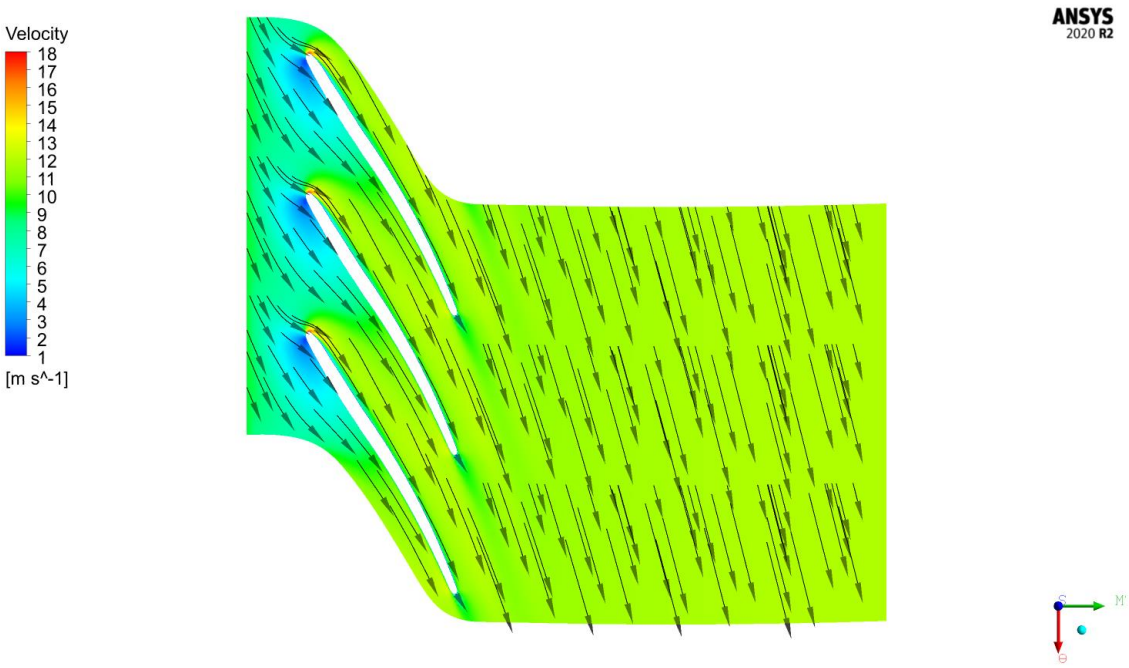


Figure 4.4: Velocity vectors at 80% span of runner

Above figure shows velocity vectors at 80% span of runner. The figure shows stagnation point at pressure side of vanes. The minimum pressure at the suction side arises from this reason. This suggest correction of guide vanes angles.

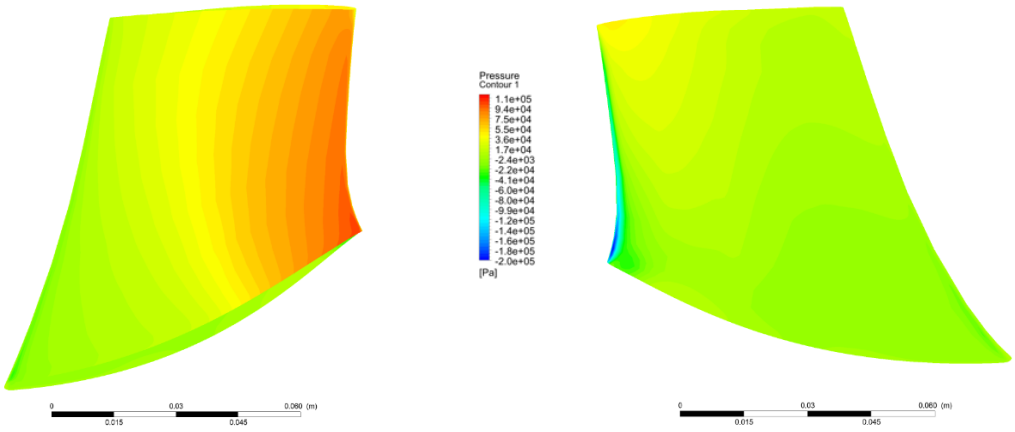


Figure 4.5: Pressure counters at the pressure and suction side of runner

Above figure shows the pressure counters at pressure and suction side of the size optimized runner. In the pressure side maximum pressure lies around the leading edge and it decreases linearly towards trailing edge. While in suction side minimum pressure is seen towards leading edge as stagnation point is seen towards pressure side. Regions after minimum pressures a linear decline of pressure is seen in suction side of blade.

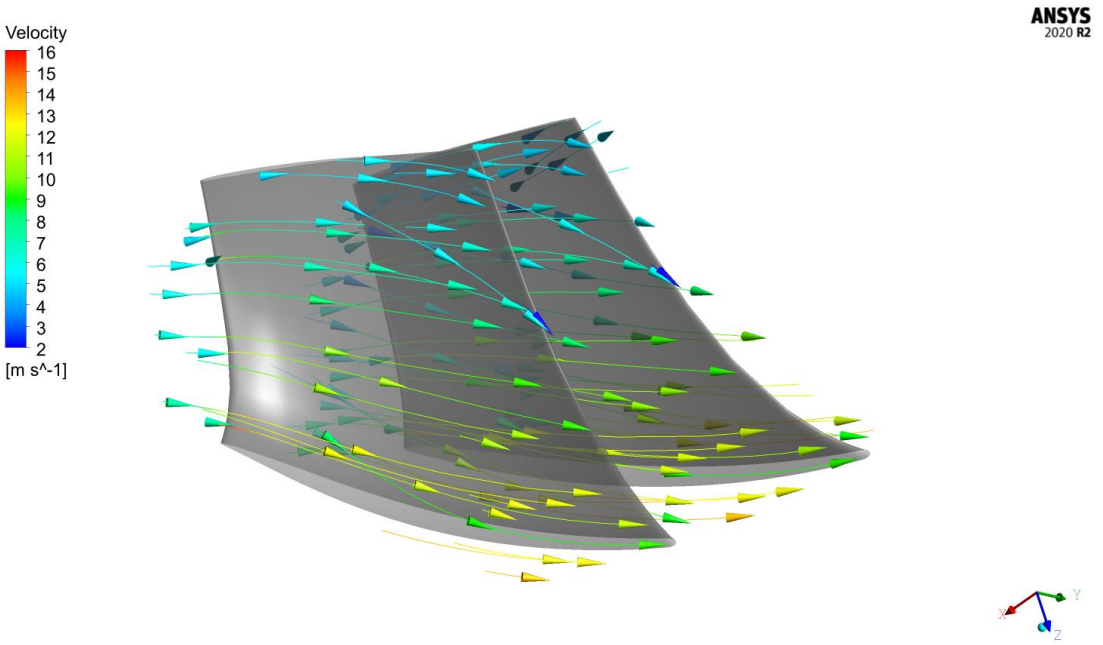


Figure 4.6: Velocity streamlines at blade span

### 4.3 Lean Angle Correction

The lean angle is defined as the blade's lean, namely, the degree of hub or shroud line shifted from the original position. The lean angle is one of the most important parameters for controlling the pressure balance in the runner.

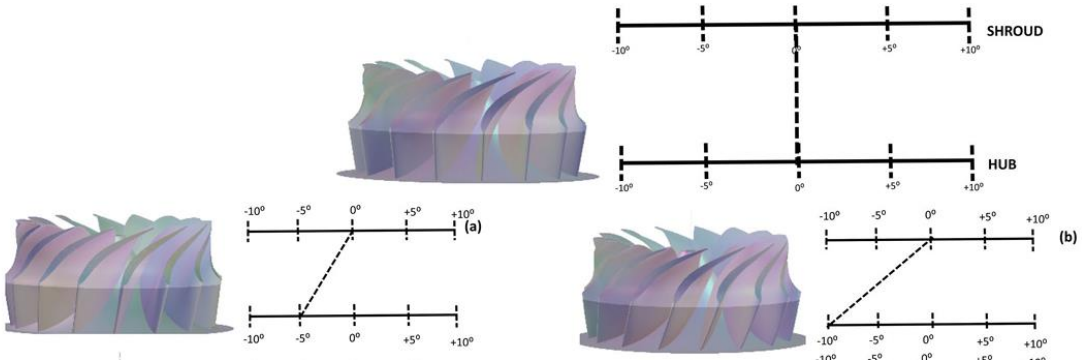


Figure 4.7: Changes of lean angle of runner

The above figure shows the effect of lean angle on shape of blades of runner (Ayli, Celebioglu, and Aradag 2016). After optimization of size of the runner lean angle correction was done. Lean angle was changed and efficiency was calculated from simulation. Lean angle of -5$^{o}$ shows maximum efficiency.

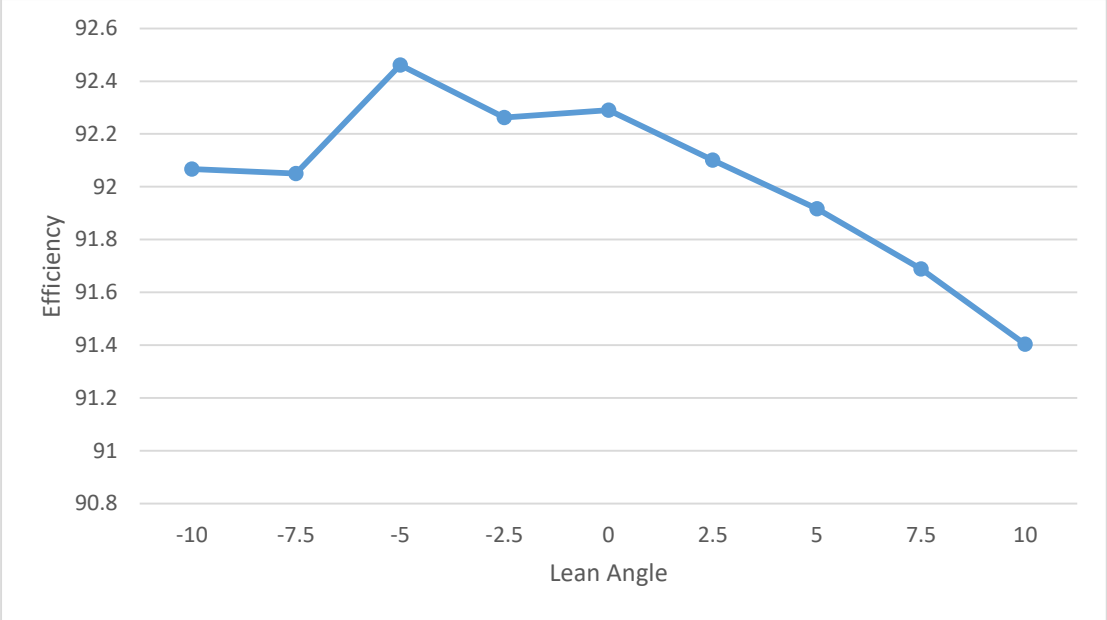


Figure 4.8: Lean angle vs. Efficiency plot

Figure 4.8 shows the plot of efficiency vs. lean angle. It was found that maximum efficiency is found at negative lean angle of 5°. General trend shows that negative lean angle performance is better than positive lean angle.

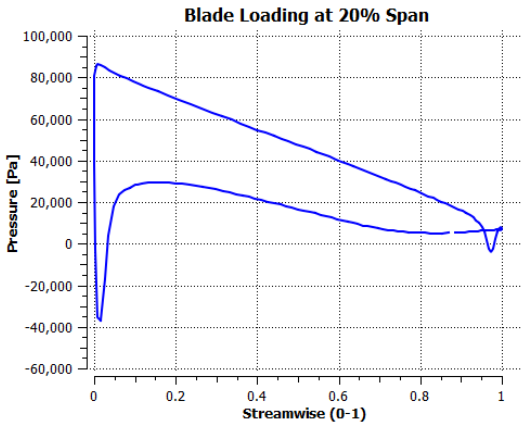


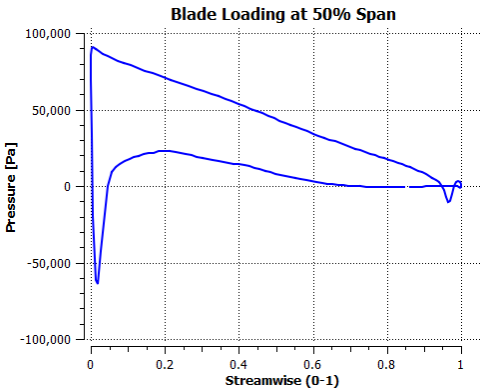


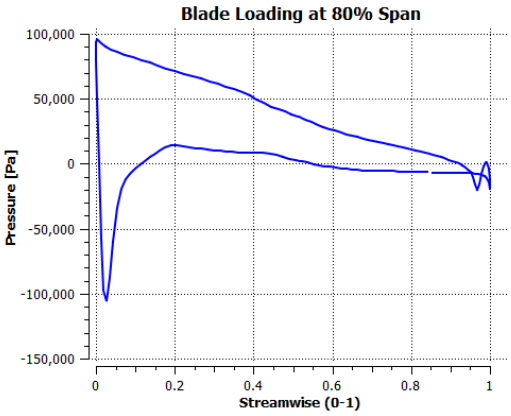

Figure 4.9: Blade loading of lean corrected runner

Blade loading shows similar pattern in lean angle corrected design and size optimized design.

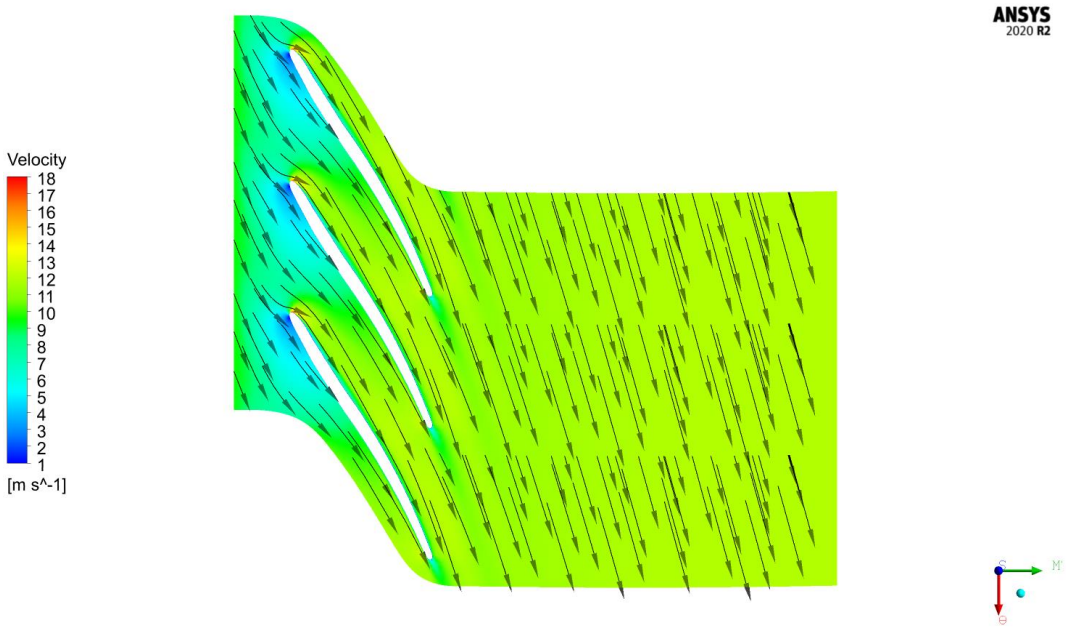


Figure 4.10: Velocity vector plot at 80% span

Figure 4.10 shows velocity vector plot at 80% span of blade. The velocity vector at the leading edges were more aligned to the blade profile so less eddies formation were seen in the velocity vector.

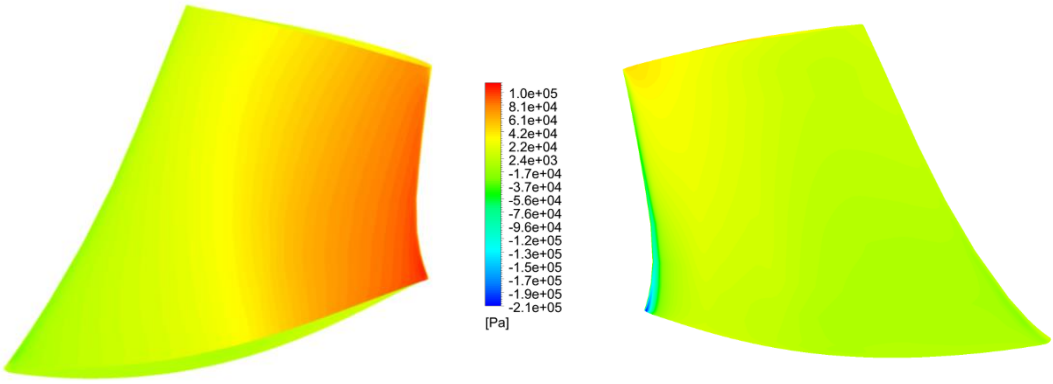


Figure 4.11: Pressure counter at pressure and suction side of lean corrected blade

Pressure counter of lean corrected blade was found to be better than size optimized Francis runner. Area containing least pressure are found to be reduced significantly on lean corrected blade.

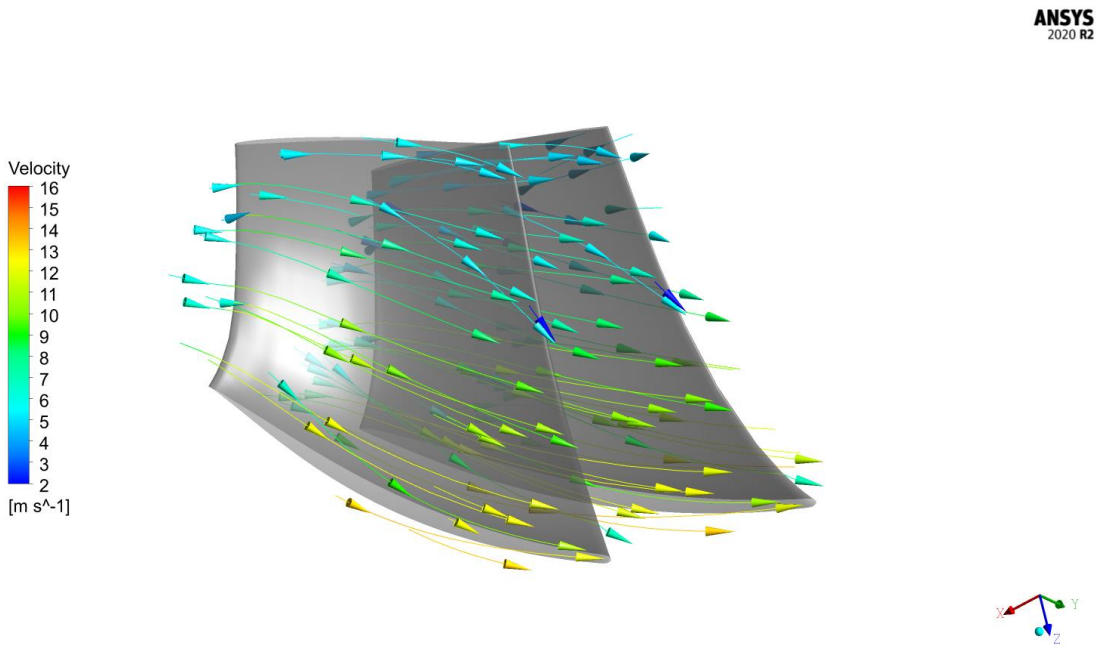


Figure 4.12: Velocity streamlines at blade surface

Above figure 4.12 shows the velocity streamlines at blade surface of lean corrected runner. Higher velocities are found to be towards shroud side and lower are found towards hub side of runner. Higher energy can be extracted from runners if leading edge is more extended near shroud region. This was also validated by (Lamichhane et al. 2021) which resulted 1.28% increase in efficiency by elongation of trailing edge near shroud region.

### 4.4 Data Screening

After size optimization and lean correction, generation of database was conducted. Six hundred initial population was selected varying the shape of meridional profile and beta distribution. After all the bgi file were generated batch simulation was conducted using Ansys CFX. Among 600 random design 578 design simulation was successfully conducted. Among them the best data is presented in data screening section.

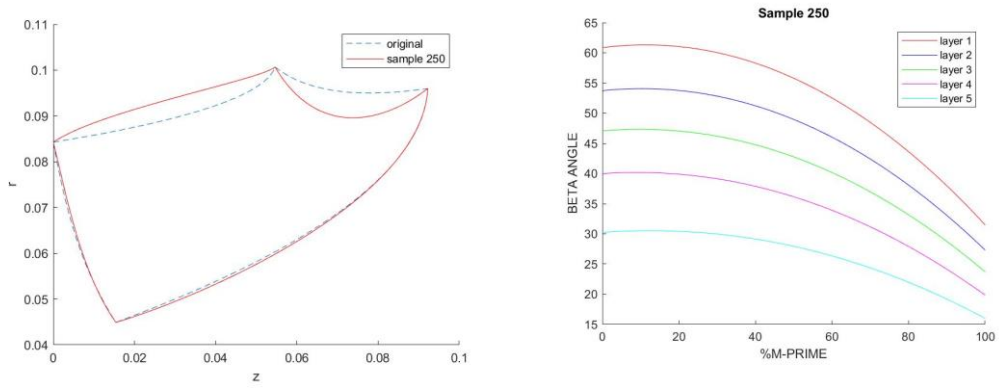


Figure 4.13: Meridional profile and beta angle distribution of screened design

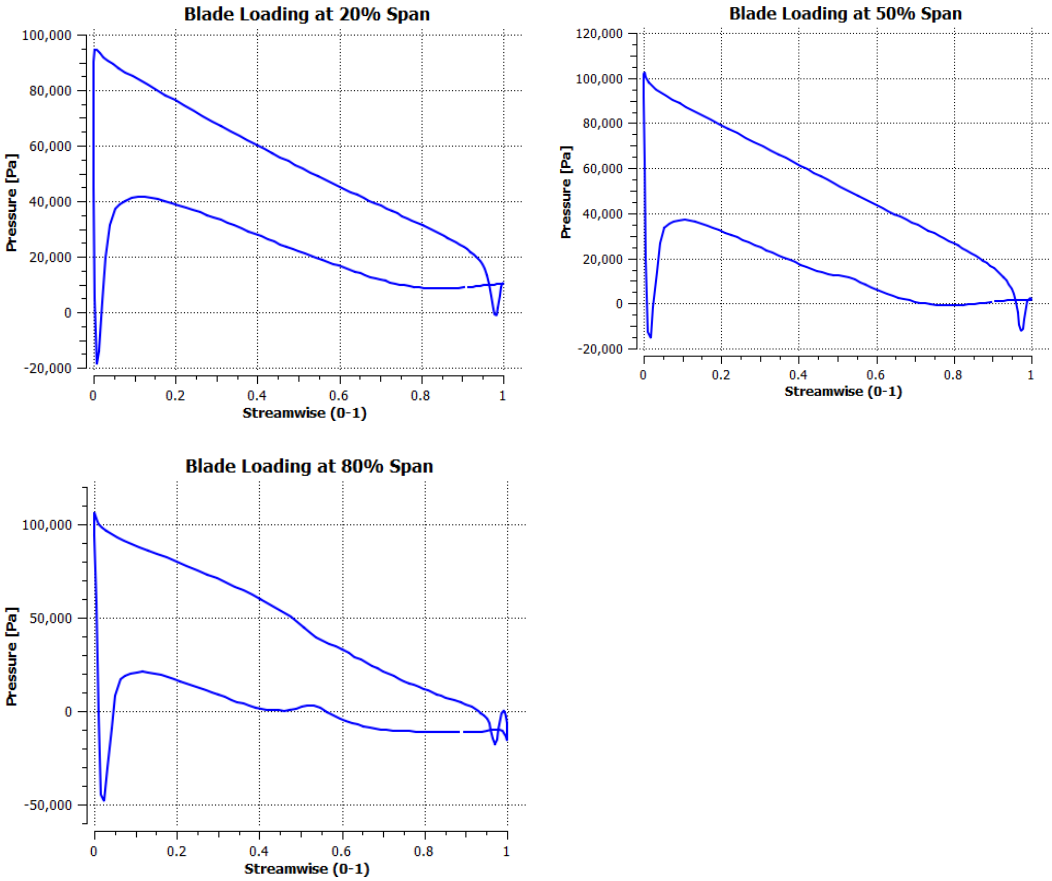


Figure 4.14: Blading loading at different span of screened blade

Above figure shows blade loading at 20, 50 and 80% of blade span. These diagram shows that energy extraction from the runner is evenly distributed.

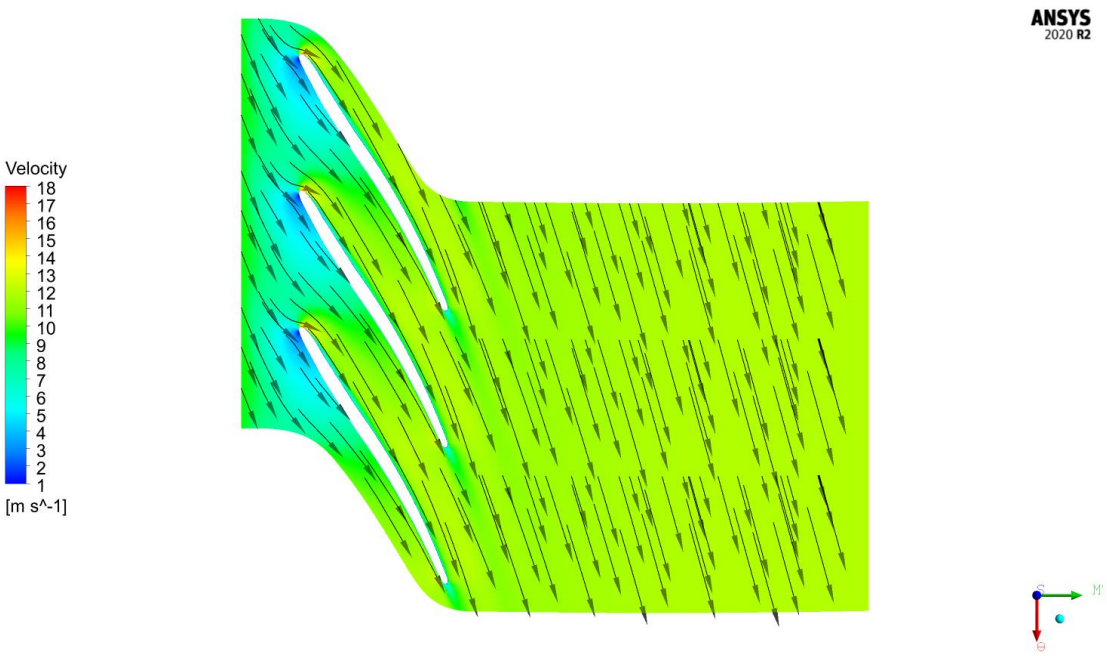


Figure 4.15: Velocity vector at 80% of span of blade

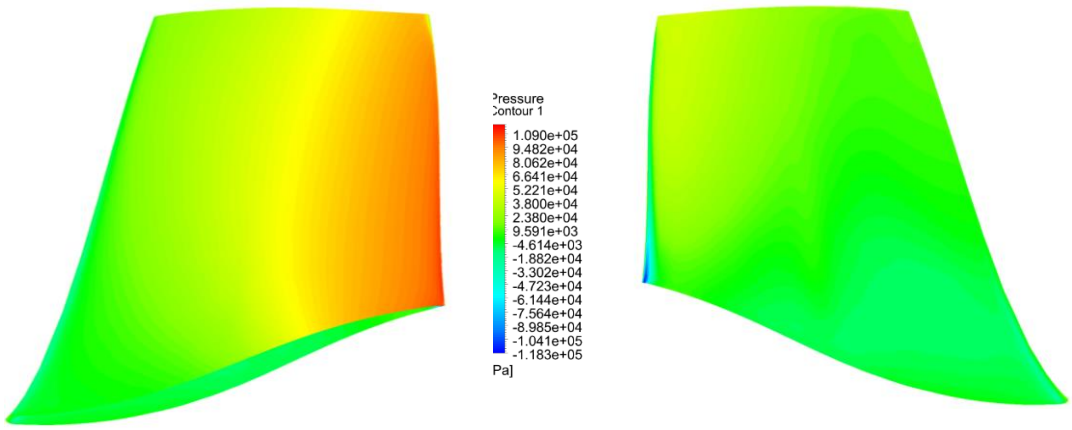


Figure 4.16: Pressure counter at pressure side and suction side of blade

Figure 4.15 and figure 4.16 shows the velocity vector and pressure counter respectively. It was found the velocity and pressure counter are improved in this case. It is evident from above figure that stagnation point has moved little towards left so that minimum pressure at the suction side of blade has decreased. Following figures shows the performance of optimized runner.

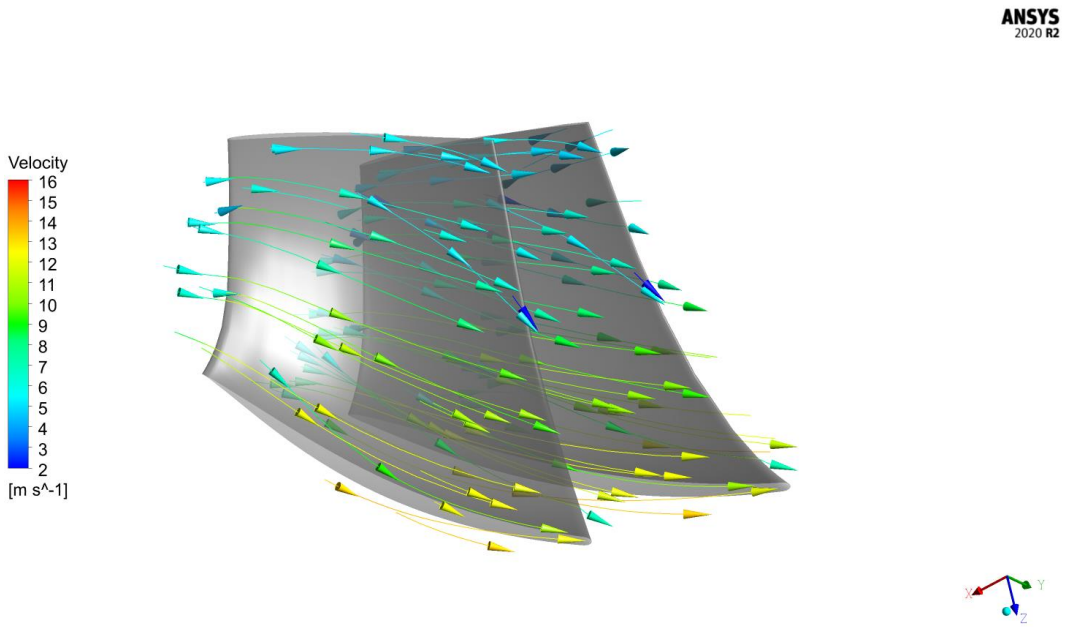


Figure 4.17: Velocity vector at blade surface

### 4.5 Optimized Runner

After the initial data was generated and simulated in Ansys CFX, it was processed for the optimization. For the optimization process first data was trained using neural network and tested. Then optimization was done using genetic algorithm.

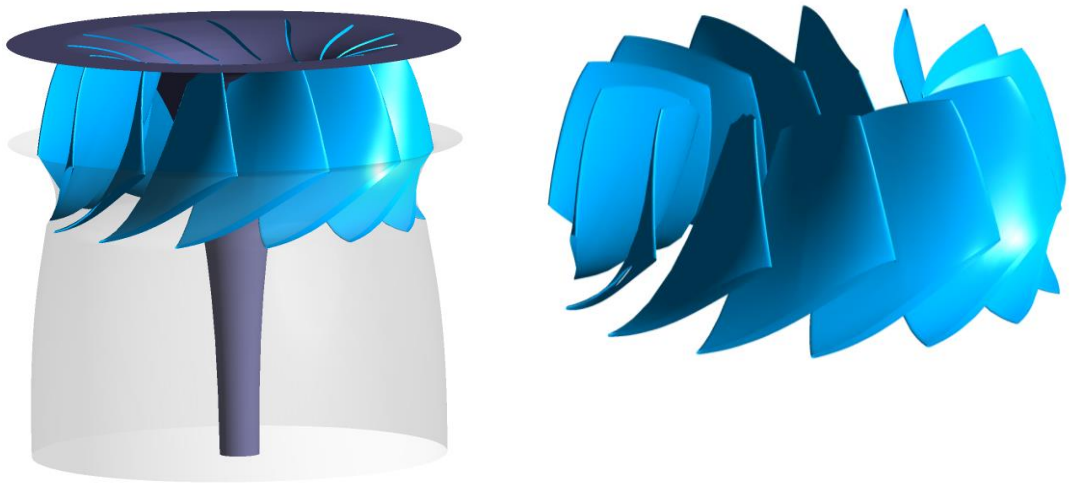

Figure 4.18: Optimized design of Francis turbine

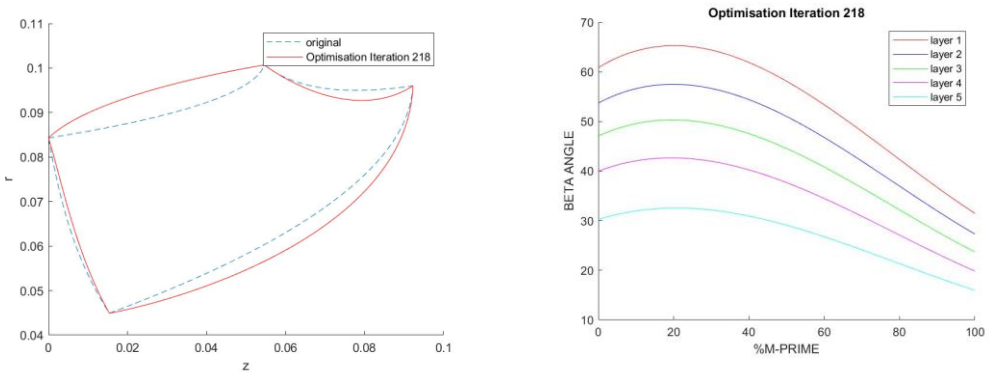


Figure 4.19: Meridional profile and blade angle distribution for optimized runner

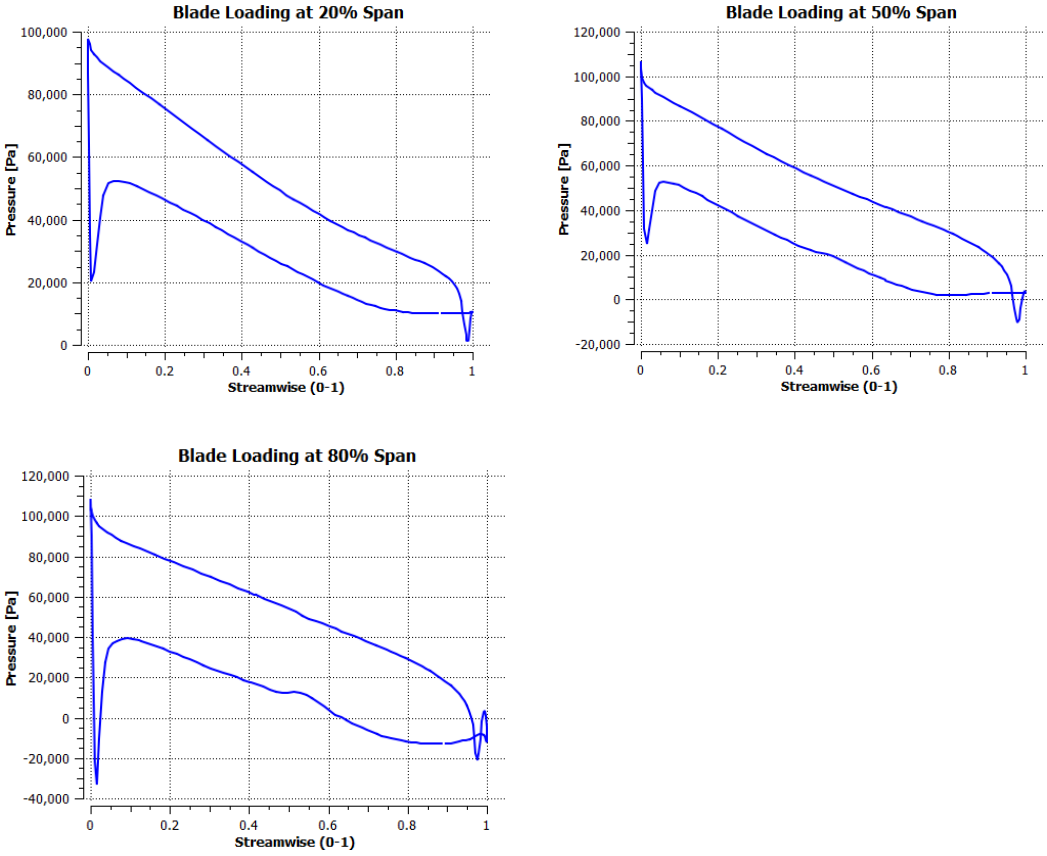


Figure 4.20: Blade loading at different span of blade

From reference design to optimized design, blading loading chart showed more uniform energy extraction.

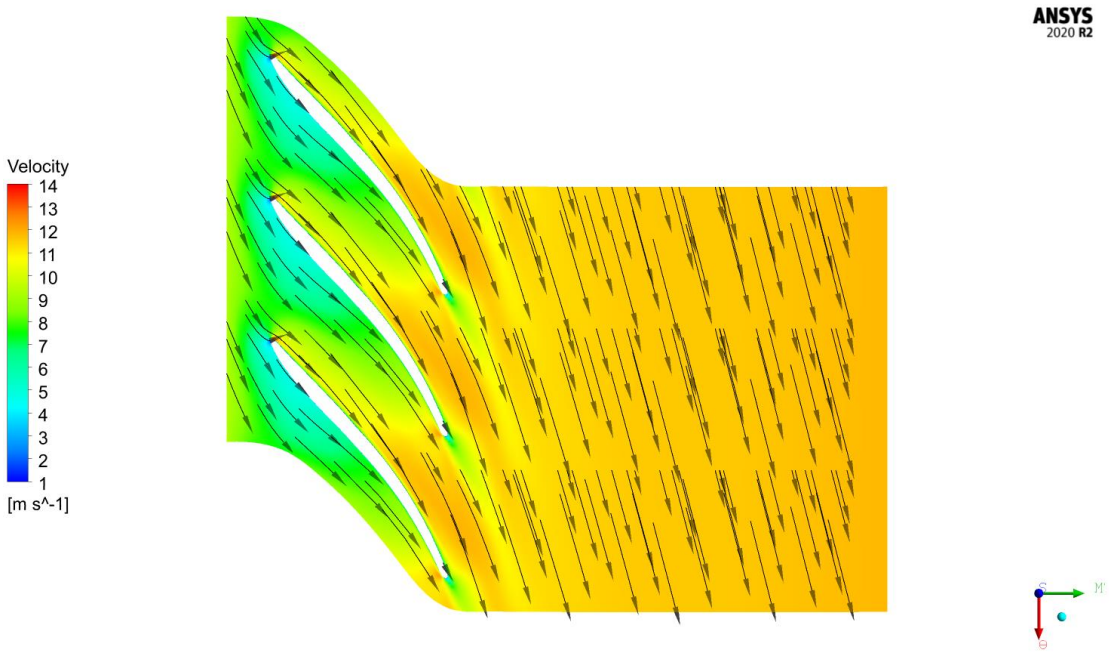


Figure 4.21: Velocity vector at 80% span

Initial interaction between water and blade is seen more better and formation of eddies is highly reduced in optimized design.

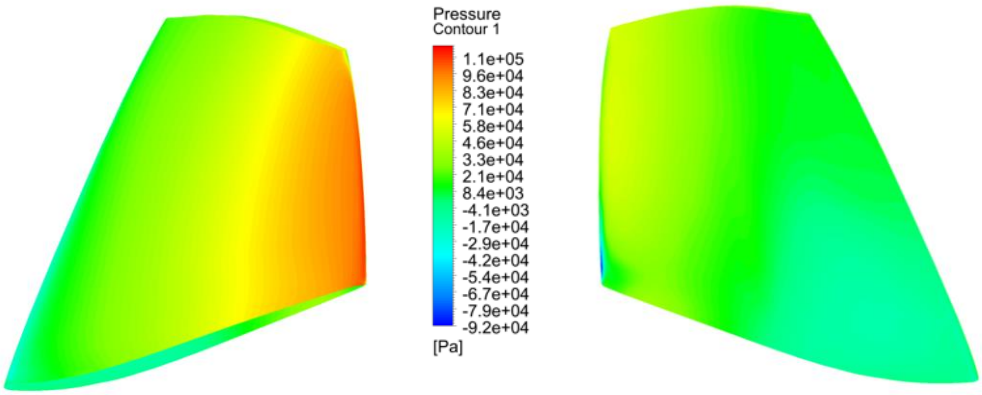


Figure 4.22: Pressure counter at pressure side and suction side

With proper alignment of velocity vector with blade profile minimum pressure at suction side has been significantly reduced.

### 4.6 Objective Function

Designing a hydraulic turbine to meet specific performance criteria is essential. To achieve this, engineers establish an objective function and constraints that encompass different design factors. The objective function represents the parameter we aim to either minimize or maximize within a given problem. Here we minimize our objective

function to find the best runner with high efficiency, with cavitation free flow, and lower erosion.

Table 4.2: Design results for initial, screened and optimized design

| Parameters | Initial design | Screened design | Optimized design |
|---|---|---|---|
| Objective Function | 0.47 | 0.4 (-14.9%) | 0.34 (-27.7%) |
| Shaft power (W) | 16226.7 | 16485.9 (1.6%) | 16252 (0.2%) |
| Efficiency | 92.4667 | 93.5075 (1.1%) | 93.6983 (1.3%) |
| Erosion tendency | 124.4 | 121.5 (-2.3%) | 102.2 (-17.8%) |
| Cavitation area | 2.2E-05 | 1.07E-06 (-95.1%) | 1.904E-07 (-99.1%) |

Table 4.2 shows the design results of initial design, screened design and optimized design. It shows in optimized design most of the reduction occurs in cavitation area. It was reduced by 99% with compared to the initial design. Shaft power and efficiency were slightly increased. Erosion tendency was reduced by 18% and objective function value was reduced by 28% with compared to the initial design.

### 4.7 Cavitation Area

During this optimization process cavitation area has reduced significantly by 99%. Cavitation area was seen on suction side of leading edge. Cavitation area was calculated by calculation the area of the runner below the vapor pressure of water at $20^{o}$. Also with the given boundary conditions of mass flow rate at the inlet and zero pressure at outlet would results in only cavitation regions on leading edge only.

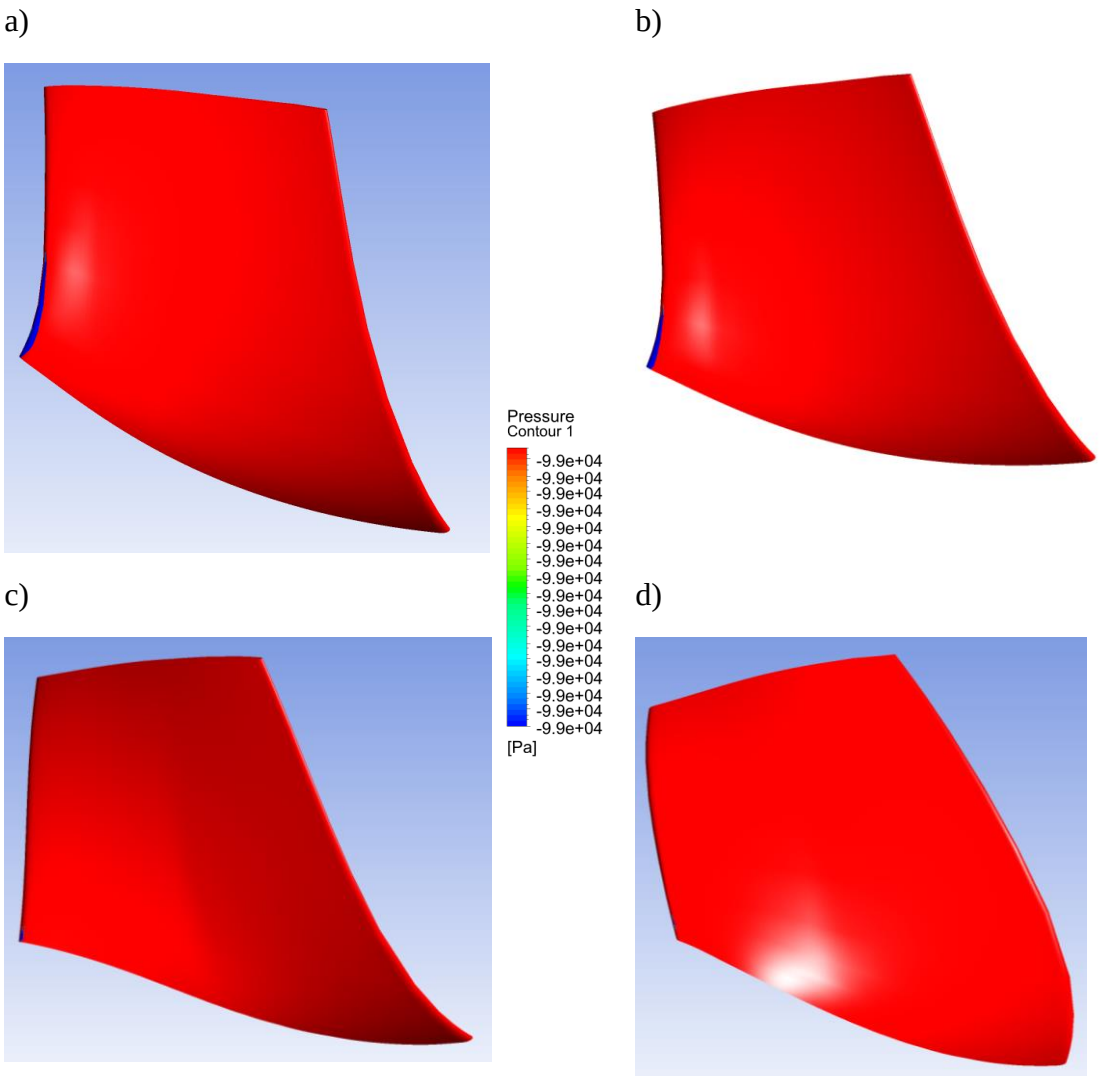


Figure 4.23: Cavitation area of a) initial design b) lean corrected design c) screened design and d) optimized design

# CHAPTER 5: CONCLUSIONS AND RECOMMENDATIONS

## 5.1 Conclusions

In this research optimization was done in three step. First size optimization, second on lean angle and finally shape optimization of meridional profile of Francis runner was conducted. Followings are the different conclusions drawn after completing this research.

- Size of a meridional profile of a Francis runner plays important role in its performance. With the given size variation minimum efficiency of 87.8% and maximum efficiency of 92.3% was achieved. The runner of maximum efficiency was chosen for further optimization
- Lean angle with -5$^{o}$ gives the best efficiency of 92.5%. With negative lean we can achieve improved part-load efficiency, reduced cavitation and enhanced flow control.
- LHS method was used to generate 600 different meridional shape design samples among which 578 designs were successfully simulated. The results from CFD simulation was used to train neural network and optimize the design using genetic algorithm.
- The optimized design shows 99% reduction in cavitation area, 18% reduction in erosion tendency and 1.3% increase in efficiency compared to the initial design. Also objective function was reduced by 28%.

## 5.2 Recommendations

Followings are different recommendations drawn after completing this research.

- Only optimization of Francis runner was conducted. Apart from the runner optimization of other components (spiral casing and draft tube) of turbine is also required.
- Full turbine simulation is required in order to validate the performance of the runner also to check the performance on off design condition.
- The obtained runner can be further simulated to check performance for erosion and cavitation

## REFERENCES


Aponte, R D et al. 2020. “Minimizing Erosive Wear through a CFD Multi-Objective Optimization Methodology for Different Operating Points of a Francis Turbine.” *Renewable Energy* 145: 2217–32.

Aradag, Selin, Hasan Akin, and Kutay Celebioglu. 2017. “CFD Based Design of a 4.3MW Francis Turbine for Improved Performance at Design and off-Design Conditions.” *Journal of Mechanical Science and Technology* 31(10): 5041–49.

Ayli, Ece, Kutay Celebioglu, and Selin Aradag. 2016. “Determination and Generalization of the Effects of Design Parameters on Francis Turbine Runner Performance.” *Engineering Applications of Computational Fluid Mechanics* 10(1): 545–64.

Baidar, Binaya, Sailesh Chitrakar, Ravi Koirala, and Hari Prasad Neopane. 2015. “Selection of Optimal Number of Francis Runner Blades for a Sediment Laden Micro Hydropower Plant in Nepal.” *International Journal of Fluid Machinery and Systems* 8(4): 294–303.

Bovet, T. 1963. “Contribution à l’étude Du Tracé d’aubage d’une Turbine à Réaction Du Type Francis.” *Informations Techniques Charmilles*.

Chen, Zhenmu, and Young-Do Choi. 2016. “A Study on the Effect of Port Area of Blade on the Performance of Francis Hydro Turbine.” *The KSFM Journal of Fluid Machinery* 19(1): 5–10.

Elikalfa, A, G Sepetci, K Celebioglu, and S Aradag. 2016. “Design of a New Francis Turbine Runner for a Rehabilitation Project in Turkey.” *Machines. Technologies. Materials.* 10(9): 11–14.

Forrester, Alexander, Andras Sobester, and Andy Keane. 2008. *Engineering Design via Surrogate Modelling: A Practical Guide*. John Wiley & Sons.

Gjøsæter, Kristine. 2011. “Hydraulic Design of Francis Turbine Exposed to Sediment Erosion.” (June): 2011.

Kaewnai, Suthep, and Somchai Wongwises. 2011. “Improvement of the Runner Design of Francis Turbine Using Computational Fluid Dynamics.” *Am. J. Eng. Applied Sci* 4: 540–47.

Kaniecki, Maciej, and Zbigniew Krzemianowski. 2016. “CFD Analysis of High Speed Francis Hydraulic Turbines.” *Transactions of the Institute of Fluid-Flow Machinery* 131(131): 111–20.

Khanal, Krishna et al. 2016. “A Methodology for Designing Francis Runner Blade to Find Minimum Sediment Erosion Using CFD.” *Renewable Energy* 87: 307–16. http://dx.doi.org/10.1016/j.renene.2015.10.023.

Kocak, Eyup, Salih Karaaslan, Nuri Yucel, and Furkan Arundas. 2017. “A Numerical Case Study: Bovet Approach to Design a Francis Turbine Runner.” *Energy Procedia* 111(September 2016): 885–94. http://dx.doi.org/10.1016/j.egypro.2017.03.251.

Lamichhane, Binaya Kumar, Hari Bahadur Dura, Laxman Poudel, and Neeraj Adhikari. 2021. “Effect of Trailing Edge Profile on Performance of Francis Turbine for Micro Hydropower.” *Proceedings of 10th IOE Graduate Conference*: 1101–9.

MILOŞ, T, and M BĂRGLĂZAN. 2004. “CAD Technique Used to Optimize the Francis Runner Design.” *6th International Conference on Hydraulic Machinery and Hydrodynamics*: 125–30. http://mmut.mec.upt.ro/mh/Conferinta_MH/212_Milos.pdf.

MUNTEAN Sebastian, Romeo F. SUSAN-RESIGA, Sandor BERNAD, Ioan Anton. 2004. “Analysis of the GAMM Francis Turbine Distributor 3d Flow for the Whole Operating Range and Optimization of the Guide Vane Axis Location.” *The 6th International Conference on Hydraulic Machinery and Hydrodynamics Timisoara, Romania, October 21 - 22, 2004* (May): 1–6.

Panta, Subash, Manish Lamsal, Bhola Thapa, and Biraj Singh Thapa. 2014. “Prediction of Turbine Needed for Future Hydropower Projects in Nepal.” *Hydro Nepal: Journal of Water, Energy and Environment* 14: 23–26.

Prasad Shrestha, Krishna et al. 2013. “Optimized Design of Francis Turbine Runner for Sand Laden Water.” *Hydro Nepal: Journal of Water, Energy & Environment* (13).

Radha Krishna, H C. 1997. “Hydraulic Design of Hydraulic Machinery.”

Sangroula, Durga Prasad. 2009. “Hydropower Development and Its Sustainability with Respect to Sedimentation in Nepal.” *Journal of the Institute of Engineering* 7(1): 56–64.

Satyal, Srijan et al. 2022. “Design and Optimization of Bovet Based Francis Runner Using Meta-Model and Genetic Algorithm.”

Shrestha, Ratna Sansar, Stephen Biggs, Scott Justice, and Amanda Manandhar Gurung. 2018. “A Power Paradox: Growth of the Hydro Sector in Nepal.” *Hydro Nepal: Journal of Water, Energy and Environment* 23: 5–21.

Shrestha, Ujjwal, Zhenmu Chen, and Young Do Choi. 2019. “Correlation of the Sediment Properties and Erosion in Francis Hydro Turbine Runner.” *International Journal of Fluid Machinery and Systems* 12(2): 109–18.

Speziale, Charles G, Sutanu Sarkar, and Thomas B Gatski. 1991. “Modelling the Pressure--Strain Correlation of Turbulence: An Invariant Dynamical Systems Approach.” *Journal of fluid mechanics* 227: 245–72.

Teran, Leonel Alveyro, Francisco Jose Larrahondo, and Sara Aida Rodr\’\iguez. 2016. “Performance Improvement of a 500-KW Francis Turbine Based on CFD.” *Renewable energy* 96: 977–92.

Wallin, Stefan. 2000. *Engineering Turbulence Modelling for CFD with Focus on Explicit Algebraic Reynolds Stress Models*. Royal Institute of Technology, Department of Mechanics Stockholm, Sweden.